Project Number DM3 - AAIE

Dosimetric Evaluation of the Fast and Thermal Neutron Facilities at the University of Massachusetts, Lowell Research Reactor

A Major Qualifying Project Submitted to the Faculty of

WORCESTER POLYTECHNIC INSTITUTE

in partial fulfillment of the requirements for the

Degree of Bachelor of Science

by

Andrew J. Daudelin

30 April 2014

Approved:

Prof. Blake H. Currier, Ph.D., Major Advisor

Prof. David C. Medich, Ph.D., Co-Advisor

1. Radiation
2. Neutrons
3. Dosimetry

Abstract

The goal of this qualifying project was to investigate the output of neutron radiation by the new fast neutron facilities at the University of Massachusetts, Lowell Research Reactor. This was done by using Monte Carlo-based radiation transport simulation software to prepare a set of dosimetric studies that were later carried out at the Lowell fast neutron facilities. A linear relationship between reactor power and particle output was found.

Acknowledgements

I would like to thank Professor Blake Currier for his guidance and support throughout this project and school year, even as he went through his first months as a father.

Thank you to Professor Dave Medich for welcoming me into his lab and offering classes that proved invaluable while working on this project.

Thank you to Professor Germano Iannaccione for introducing me to the folks at the WPI radiation lab.

Thanks also to Steve Snay, Leo Bobek, and the staff of the University of Massachusetts, Lowell Research Reactor for granting access to the reactor facilities and giving me a great chance to do some really cool experiments.

A big thank you to my parents for their support throughout this and every year.

Finally, shout outs to boots and also to cats. All-nighters are easier with good music.

Executive Summary

Nuclear science is a popular area of study with many applications in the fields of research and energy: 104 nuclear power plants and 54 research reactors were active in the United States alone as of 2011 [1, 19]. The reactor at the University of Massachusetts, Lowell is one such research reactor. In order to perform experiments using its recently installed fast neutron facility, it is essential to understand the output of particles from the reactor at various power settings.

The goal of this major qualifying project (MQP) was to investigate the output of neutron radiation by the University of Massachusetts, Lowell Research Reactor (UMLRR), and to independently evaluate the safety of the reactor facilities. Monte Carlo-based computational models were used to simulate different physical geometries and the behavior of neutron radiation therein. The data obtained from the simulations was used to plan a study of the fast neutron facilities at the UMLRR. In this study, dosimeters were exposed to radiation at the fast neutron facility and measured the photon and neutron dose. The recorded dose is directly related to particle fluence.

The dosimeters used aluminum oxide thermoluminescent detection material for photon detection, and CR-39 polyethylene material, which records ion tracks caused by interactions with neutrons of energies between 40 keV and 40 MeV, to measure neutron dose [11]. Dose measurements were taken for four different reactor power settings for varying lengths of time to establish a relationship between reactor power and recorded dose rate.

A linear correlation was found between the power setting of the reactor and the combined gamma and neutron dose rate recorded by the dosimeters. It can be concluded that the fluence rate of particles increases linearly with reactor power, though more data is required to establish an exact relationship.

Table of Contents

List of Figures

List of Tables

Introduction

With 104 nuclear energy plants and 54 research reactors present in the United States alone as of 2011 [1, 19], nuclear energy and experimentation is never far from the public spotlight. From military to medicine, nuclear science is an ever-present facet of modern research and technology.

Research reactors are used for a variety of purposes, many involving neutron generation [19]. The neutrons produced by the nuclear processes in the reactor core can be moderated to a desired energy and then directed for various uses. One such use is neutron imaging, where a neutron beam is used like an x-ray to view the internal structure of an object, is a common procedure at many research reactors. Neutron imaging can be used to evaluate the structural integrity of materials under a variety of conditions down to the atomic level and with greater clarity than other methods, making it an exciting field of research.

Another common use of research reactors is the creation of radioactive materials for use in industry and medicine through neutron activation, where stable elements are exposed to and absorb low-energy "thermal" neutrons. One example in the field of medicine is irradiation of ytterbium-176. This process yields ytterbium-177, which in turn decays rapidly to lutetium-177, a radioisotope often used for radiation therapy in cancer treatments. Neutron activation can also be used to identify the component elements of unknown materials, as activated materials will emit distinct radiations based on their composition.

The University of Massachusetts Lowell Research Reactor (UMLRR) is a pool-type research reactor, with its core submerged in a 35-foot deep water pool for cooling and shielding purposes. The reactor is capable of producing one megawatt of power at peak output. Neutrons from the reactor can be moderated to lower energies, on the scale of 0.01 eV, for use in neutron activation and neutron imaging experiments. This takes place in the thermal column, where moderating materials slow the neutrons through collisions with atomic nuclei.

Only recently has the reactor been outfitted with components that make experiments with fast neutrons with energies on the scale of 1 MeV. The plate-type low-enriched uranium fuel used in the reactor allows for high neutron fluence rates of over 10^{11} neutrons per square centimeter per second [24]. It is important to gather as much data as possible on the output of the

reactor's fast neutron facilities in order to properly evaluate its capabilities and the risk it may pose to operators. The reactor facilities can only be made safer with more information.

The main goal of this project was to characterize the thermal column and fast neutron facilities at the University of Massachusetts, Lowell using a combination of computational simulations of radiation transport, dosimetric readings taken at the reactor, and activation experiments performed on-site. Characterization of the neutron facilities began with simplified models made using Monte Carlo Neutral Particle Transport Code (MCNP). These models were used to study the relationship between neutron energy and absorbed dose of neutron and gamma radiation. The models were also used to investigate the efficacy of introducing a solid water backing to dosimeters in order to more accurately simulate dose that would be received by a human.

An experiment performed at the fast neutron facilities consisted of exposing neutron- and photon-sensitive dosimeters to the radiation produced by the reactor at various energies and for varying lengths of time. The dosimeters contained aluminum oxide thermoluminescent material for recording photon dose and CR-39 polyethylene for recording neutron dose. This experiment resulted in dose and dose rate readings which were compared to the MCNP simulations to better understand the capabilities of the reactor.

The data gathered with this series of experimentation on the neutron facilities at UMass Lowell will be highly useful in evaluating their capabilities and safety. When working with potentially hazardous radioactive material in a high-powered environment like a reactor, especially one with relatively new facilities, it is good to have a much information about your system as possible. Furthermore, the procedures performed could easily be reproduced at any comparable reactor to produce actionable data and help make nuclear facilities around the world safer.

Background

Radiation and Dosimetry

Radioactivity arises in nuclei that are energetically unstable, due to an irregular neutron-proton ratio or because the nucleons are not in a ground state. For example, carbon-12 is a nucleus with 6 protons and 6 neutrons and is stable. A possible isotope of carbon with two additional neutrons, carbon-14, is not stable and will transform into the stable isotope nitrogen-14 by emitting a beta particle. Radioactive isotopes are also referred to as radionuclides.

Nuclear Transformations

Different transformations can occur depending on how unstable a nucleus is. A nucleus with a neutron-to-proton ratio that is too high to be stable can emit a β^- particle, an electron, to reduce the ratio and emit energy in the form of the electron's kinetic energy.

When a nucleus has a low neutron-to-proton ratio and needs to release a high amount of energy, it will emit an alpha particle, comprised of two protons and two neutrons. If it needs to release a lower amount of energy, it can emit a β^+ particle, a positron. If the nucleus is not energetic enough for even that, it can undergo electron capture, where an orbital electron is absorbed into the nucleus to reduce the neutron-proton ratio, and then emit a photon to shed energy.

Many, if not all, nuclear transformations result in the nucleons having a more energetic configuration than the ground state. An excited nucleus will naturally shed energy and transition to a lower energy state by either emitting a photon, or by imparting energy to an orbital electron and thereby ejecting it.

In each of these transformations, the emitted particles have enough energy that they could eject electrons, protons, or neutrons from atoms that they interact with. As such, alpha, beta, and gamma are known as ionizing radiations. The effects these radiations can have on other atoms can break chemical bonds or cause the formation of highly reactive ions. In materials this can cause a breakdown of the atomic structure; in living tissue, it can lead to cell death or the creation of cancerous cells.

Activity

The number of transformations a group of radionuclides undergoes per unit time is known as its activity. The SI unit for activity is the Becquerel (Bq), equivalent to one transformation per second. Another common unit of activity is the curie (Ci), equivalent to 3.7×10^{10} Bq.

The activity of a given radionuclide is proportional to the amount of the nuclide present:

$$A = \lambda N \quad (1)$$

As a radionuclide transforms into more stable nuclides over time, the number of atoms of the original nuclide decreases exponentially. This means that the activity of the sample due to that nuclide also decreases:

$$N = N_0 e^{-\lambda t} \quad (2)$$

$$A = \lambda N_0 e^{-\lambda t} \quad (3)$$

The proportionality constant λ is known as the decay constant, and is specific to each nuclide.

Radioactive transformations on the atomic level are entirely stochastic; that is, it is impossible to say when a given unstable atom will transform. On a macroscopic level however, radioactive elements have a half-life, the amount of time it takes for half of the atoms of a radionuclide to transform. Half-life is inversely proportional to the decay constant, as $T_{1/2} = \frac{\ln 2}{\lambda}$.

Radiation Quantification

Dosimetry refers to the measurement of radiation dose received by material or tissue due to exposure to ionizing radiation. Radiation is seen by many as a highly dangerous toxicant, responsible for radiation poisoning, cancer, and a number of other less-than-desirable maladies. The truth is that, while radioactive material can be dangerous if mishandled or misused, radiation is quite simple to detect. Its effects are well-known and very small doses can be measured.

There are a variety of ways to quantify radiation levels. The first way radiation was ever quantified, a value known as exposure, is the measurement of ionization caused by photons in

air, commonly measured in roentgen (R), equal to $2.58x10^{-4}$ coulombs per kilogram of air, or 1 electrostatic unit per cubic centimeter. This type of measurement was designed to measure photon radiation in air specifically. Many types of radiation detectors are gas ionization chambers that use this type of measurement to give the user an idea of the radiation activity and energy in an area.

A more ubiquitous measurement is absorbed dose, which quantifies the amount of energy imparted to a material by ionizing radiation. The unit of absorbed dose is the gray (Gy), defined as one joule per kilogram. Since absorbed dose is measured in energy per unit mass, any given point in an object—not necessarily the object as a whole—can be assigned an absorbed dose.

Radiation Interaction with Matter

Radiation interacts with matter in a variety of ways depending on what type of radiation it is. In particular, uncharged particles—photons and neutrons—interact very differently from charged particles such as beta and alpha particles. Charged particles interact through Coulombic forces, leading to what is known as direct ionization. Uncharged particles cause indirect ionization through nuclear interaction. In general, uncharged particles interact with materials far less than charged particles. This means that uncharged particles penetrate further into any material they encounter [22].

Photons may be produced either in an atomic nucleus or in the electron cloud surrounding it. When an excited and unstable nucleus collapses to a more stable configuration, a photon will be emitted as the carrier of the energy difference. Photons emitted from an atomic nucleus are known as gamma rays. Photons may also be emitted by electrons in an atom which move to a lower energy state; the difference in energy is released as a photon. Regardless of their origin, these photons can have a wide range of energies. The distinction between gamma rays and non-gamma photons is made because gamma photons are created with characteristic energies that can provide information on the atom from which it came.

Photon interaction with matter has three main modes: photoelectric absorption, Compton scattering, and pair production [22]. Photoelectric absorption occurs when a photon is entirely absorbed by an atomic electron. With the energy from the photon, the electron will be raised to a

higher-energy orbital or may be ejected from the atom entirely (Figure 1). An ejected electron will go on to have further interactions with the material and is an example of secondary radiation. This photoelectric effect is most common with photon energies lower than 0.1 MeV.

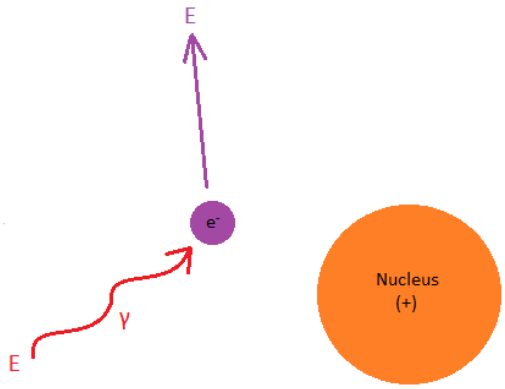

Figure 1 - In photoelectric absorption, an atomic electron fully absorbs the energy of an incident photon.

Compton scattering is the dominant effect with photons with energies between 0.1 MeV and 1 MeV. Compton scattering occurs when an incident photon interacts with an atomic electron and imparts a portion of its energy sufficient to eject the electron from the atom. The result is a secondary electron and a lower-energy photon which propagate at an angle to one another that may be related back to the initial energy of the photon. Both the lower-energy photon and the secondary electron will go on to have further interactions (Figure 2).

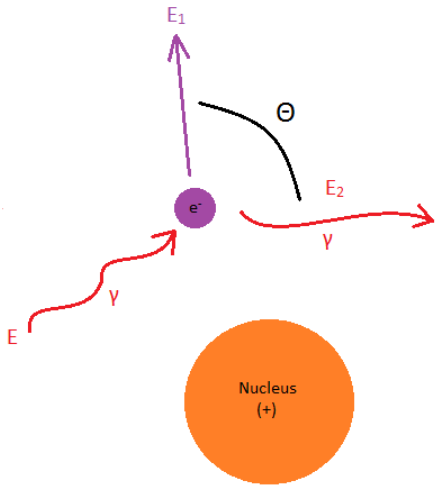

Figure 2 - In Compton scattering, the incident photon is not fully absorbed by the atomic electron. The angle between the scattering electron and photon is related to the photon's initial energy.

When a very high energy photon comes under the influence of the electromagnetic field of an atomic nucleus, it may be converted into an electron-positron pair. Electrons and positrons both have a rest mass of 511 eV; thus the original photon must have an energy of at least 1.022 MeV, the sum of the rest energies of the resulting particles. All energy in excess of the required 1.022 MeV is divided equally between the pair as kinetic energy, and the particles will propagate in exactly opposite directions (Figure 3). Both particles will interact with surrounding matter through electromagnetic forces until they shed sufficient energy. The electron may be captured by an atom, whereas the positron will encounter another low-energy electron and be annihilated.

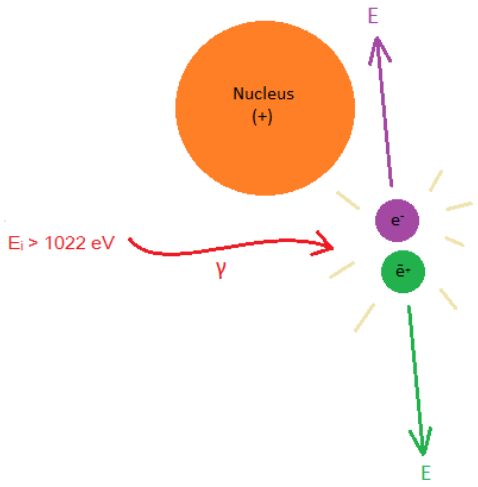

Figure 3 - In pair production, a high-energy photon under the influence of an atomic nucleus is converted into an electron-positron pair. The resultant particles propagate in exactly opposite directions.

Neutrons interact with matter by colliding directly with the nucleus. When a neutron collides with an atomic nucleus, it will scatter elastically and possibly impart enough energy to knock free a neutron or proton. If a neutron is knocked free, it will continue on much like the original incident particle, albeit with a lower energy. The recoiling atom can also collide with surrounding particles. Once a free neutron reaches a low enough energy, it may be captured by a nucleus, possibly resulting in a nuclear reaction.

A freed proton will interact as a charged particle with atomic electrons. Through Coulombic forces the proton can impart some of its energy to an electron, which may be enough to free it and ionize the atom. Even if the electron is not freed, it will be greatly excited and emit a high-energy photon when it falls back to a stable energy level.

Thermoluminescent Dosimeters

Thermoluminescent dosimeters (TLDs) are radiation dosimeters which measure dose using crystal structures, commonly calcuim fluoride or lithium fluoride, with intentional impurities (called a dopant, or doping material) to capture excited electrons in excited energy states. When the TLD is exposed to ionizing radiation, electrons are excited to higher energy states. Normally they would fall back to ground state quickly, but the impurities in the crystal structure trap the electrons in the excited state [21].

To measure the dose recorded by the TLD, the dosimeter is heated, which relaxes the crystal structure and allows the trapped electrons to fall back to ground state by emitting photons. The photons emitted are measured and related to the radiation dose received.

TLDs are mainly used to measure beta and gamma radiation. Various metal foils can be used to filter the type of radiation that reaches the dosimeter. The material used in the TLD affects what type of radiation it will record. For example, a lithium fluoride detector can detect gamma and neutron dose since neutrons will interact with the lithium and produce an alpha particle that will interact with electrons in the crystal lattice. A calcium fluoride TLD will not detect neutron radiation since neutrons do not readily interact with heavy calcium atoms and are similarly unlikely to interact with electrons directly since neutrons are uncharged.

The thermoluminescent material in the dosimeters used for the experiments at the Lowell reactor was aluminum oxide that was formulated to contain carbon impurities (Al_2O_3:C).

Neutron Dosimetry

An effective way to measure neutron radiation dose is to use allyl diglycol carbonate, commonly known as CR-39. CR-39 is a polyethylene resin that has been used to make lenses and eye protection. When pure CR-39 is exposed to neutron radiation, neutrons can interact with the hydrogen atoms in the resin to cause protons to recoil with great energy [5]. These cause ion tracks to be etched into the material. In dosimeters containing boron, a reaction which releases an energetic alpha particle also leads to ion tracks. Just as with TLDs, metal filters can be used to

block neutrons of certain energies. For example, cadmium is a strong absorber of low-energy neutrons, so it is used when fast-neutron dosimetry is desired.

To measure the dose, the CR-39 material is etched, commonly with sodium hydroxide, to enlarge the tracks. The tracks are then optically analyzed to evaluate the dose.

Where TLDs are insensitive to neutron radiation, CR-39 does not detect gamma or beta radiation. A combination of a TLD chip and CR-39 material are used to make dosimeters which are useful for measuring a variety of radiation.

The dosimeters used in the experiments at the Lowell reactor contained CR-39 material for recording neutron dose. The CR-39 detected neutrons with energies between 40 keV and 40 MeV.

Radiation Weighting Factors and Dose Limits

Since radiations differ in both physical makeup and interaction mechanism, some types are more damaging than others. An alpha particle has twice the charge and almost 2000 times the charge of a beta particle, so it is to be expected that an alpha particle will interact more and with greater effect than a beta.

One metric used to quantify the difference between radiations is linear energy transfer (LET), which is the amount of energy transferred by a particle's interactions per unit length of its track. LET is commonly measured in units of keV/μm [6]. In general, LET is proportional to particle mass and charge, and inversely proportional to particle energy: high energy particles will have fewer interactions per unit track length than slower particles.

Another consequence of the differences in energy deposition by various particles is a difference in how much impact they will have on a biological system. This difference is quantified using relative biological effectiveness (RBE). RBE is calculated by finding the dose D_{250} of 250 kVp photons (photons created with a source of 250 kV potential) required to cause a given biological effect, and the dose D_r required of a test radiation to cause the same effect. The relative biological effectiveness of the test radiation is the ratio of these two values [6]:

$$RBE = \frac{D_{250}}{D_r} \quad (4)$$

RBE and LET are not directly related because of the nature of the critical target in biological cells. Relative biological effectiveness increases with linear energy transfer up to an LET of around 100 keV/µm. At this point, the average distance between ionization events is equal to the width of the DNA double helix, and the radiation is most likely to cause a double strand break in the DNA, which is the main cause of most biological effects in living organisms. Above 100 keV/µm, RBE falls off rapidly. This is because there are more ionization events than required to sufficiently damage the DNA, meaning energy is wasted.

There are many complex differences in relative biological effectiveness of different types and energies of radiation, so it is necessary to use a more generalized quantification system. A radiation weighting factors (w_R) is now commonly used, based on RBE studies as well as a variety of other consideration. In these systems, low LET radiation such as photons and electrons have weighting factors of one. Alpha particles have the highest weighting factor at 20. High-energy proton radiation has a weighting factor of 2. Neutron radiation has a highly variable biological effectiveness based on particle energy, so a continuous function is used to relate energy with weighting factor [17]. Discrete values can be used when precision is not required.

Table 1 - Radiation weighting factor by particle type and energy [25]. The values for neutron radiation are from ICRP Publication 60 [20] and are accurate for approximation.

Radiation Type	Particle Energy	Weighting Factor w_R
Photon	All	1
Beta (electron, positron)	All	1
Proton	>2 MeV	2
Neutron	<10 keV	5
	10 keV – 100 keV	10
	100 keV – 2 MeV	20
	2 MeV – 20 MeV	10
	>20 MeV	5
Alpha, Heavy Ion	All	20

These radiation weighting factors are used as dose multipliers to calculate an effective dose E. While the unit of absorbed dose is the gray (Gy, equal to 1 J/kg), the units of effective dose are the Sievert (Sv). To obtain an effective dose value, the absorbed dose is multiplied by the weighting factor of the radiation involved:

$$E = w_R \cdot D \tag{5}$$

Thus an absorbed dose of 1 Gy of photon radiation is an effective dose of 1 Sv. However, 0.5 Gy of proton absorbed dose is an effective dose of 1 Sv because the proton weighting factor is 2.

In order to protect workers in the radiation industry—engineers, laborers, medical radiologists, and anyone else who regularly comes into contact with radioactive materials—as well as the general public, regulatory committees have set dose limits for both workers and the public. The International Commission on Radiological Protection (ICRP) sets the occupational dose limit for whole-body dose at 0.02 Sv per year, averaged over 5-year intervals. The recommended limit for the public is 0.001 Sv per year.

Table 2 – Annual dose limits set by the ICRP and US NRC [9, 13].

Type of Limit	**International Commission on Radiological Protection**		**US Nuclear Regulatory Committee**	
	Occupational	*Public*	*Occupational*	*Public*
Effective Dose	0.02 Sv*	0.001 Sv	0.05 Sv	0.001 Sv
Eye Lens	0.15 Sv	0.015 Sv	0.15 Sv	--
Skin	0.50 Sv	0.05 Sv	0.50 Sv	--
Extremities	0.50 Sv	--	0.50 Sv	--

*To be averaged over a five-year period, with provision that dose should not exceed 0.05 Sv in any one year.

Limits for dose to the eye lens and skin are specified because those tissues are not necessarily protected by the limit put on whole body dose.

Although the standing theory is that any radiation exposure will increase cancer risk, these limits have been determined to provide sufficient protection.

Biological Effects of Radiation

Ionizing radiation interacts with living cells primarily by damaging cell DNA. While radiation can interact with and damage other parts of a cell, it has been shown that relatively high doses are required for a biological effect to arise due to this type of damage (on the scale of gray); whereas irradiation of the cell nucleus leads to biological effects at much lower doses, on the scale of centigray [6]. While a single "hit" by radiation of sufficient energy can cause a strand break in the DNA chain, many interactions are required to cause sufficient damage to cell organelles to lead to cell death. Note, however, that thanks to the redundant structure of many chromosomes (human chromosomes contain two copies of genetic information, for example), more than one strand break is required to cause biological effects.

Sufficient damage to the DNA chain in the nucleus of a cell can lead to aberrations in the structure of the chain, which, if not properly repaired by cell mechanisms, can lead to abnormal cell duplication or clonogenic death, where the cell is unable to divide properly. In the former case, abnormal cell growth can lead to cancer. In the latter, acute doses of radiation can cause cell death. A localized dose will cause topical effects such as hair loss or skin reddening, while whole-body dose will lead to the symptoms of acute radiation sickness.

Some types of cells are more radiosensitive than others. Radiosensitivity is dependent on a number of factors, including cell activity and division rate, cell age, and cell specialization. Acute radiation sickness is presented according to these sensitivity factors. At relatively low doses, sickness presents itself over a longer time scale because only young cells are affected: symptoms will not arise until the current population of cells dies out naturally. At higher doses, more cells are affected and symptoms are more prompt and severe. The concept of a 50% lethal dose (LD_{50}) is used in the context of high-dose acute irradiation. The $LD_{50/60}$ is the dose at which 50% of individuals exposed will survive the 60 days following irradiation. If an individual survives past 60 days, the body will have mostly recovered from the cell death caused by radiation and is expected to survive.

The organs that are responsible for the creation of blood are the most radiosensitive [6]. Stem cells purposed for replenishing blood cells are active, young, and unspecialized, and are thus the first to die when exposed to radiation. Doses as low as 0.15 gray can affect blood count, and doses around 0.5 gray will affect white blood cell levels within a number of minutes.

Organs in the digestive system are the next most radiosensitive life-critical organs [6]. Again, it is the stem cells that will replace the linings of the stomach and intestines that are most severely affected. Doses of 5 gray or more will cause degeneration of the digestive organ cells within hours.

The biological effects of acute radiation exposure area as follows:

Table 3 - Biological effect on humans of radiation dose [16]. Marked symptoms can occur after localized radiation exposure, not just a whole-body dose.

Dose (cGy)	Effect
15 - 25	Possible blood count changes
50	Certain blood count changes
100	Vomiting
150	Death threshold
320 – 360	$LD_{50/60}$ with no medical care *Epilation (hair loss) *Erythema (skin reddening)
480 - 540	$LD_{50/60}$ with medical care

Below a 1.5 gray dose, symptoms are similar to a viral sickness: fatigue, nausea, and vomiting. The cell death caused by radiation is recognized by the body as a biological infection and it responds as such.

Above 1.5 gray, a dosed individual will have low counts of red blood cells, white blood cells, and platelets. Infection is the most serious risk at this point, and hemorrhaging is another major concern. Isolation, antibiotics, and blood transfusions will increase likelihood of survival. Doses high enough to effectively wipe out blood production cells will require a bone marrow transplant for survival to be possible.

Radiation doses above 5 gray may wipe out the gastrointestinal tissues. At this point, the body can no longer absorb nutrients or protect itself from bacteria in the intestines, and death is certain.

A full-body dose above 20 gray will affect even the most radioresistant tissues in the muscular and nervous systems. Rapid death is all but certain, often due to edema. Interestingly, much higher doses are required to cause death if dose is limited to the head region alone. The reason for this is not well understood [6].

While lower doses will not lead to non-stochastic effects such as the acute symptoms described above, it is thought that any dose is liable to increase an individual's risk of developing cancer [7]. Unfortunately, this stochastic effect is difficult to quantify.

Much of the data regarding radiation-induced cancer is from the survivors of the atomic bomb strikes on the Japanese cities of Nagasaki and Hiroshima, and the Chernobyl reactor meltdown. The A-bomb survivors were exposed at high dose rates to gamma radiation and a smaller component of neutron radiation. Chernobyl survivors, mainly those who were subject to fallout from the disaster, were exposed to a variety of radioactive isotopes, with the beta and gamma-emitting iodine-131, strontium-90, and cesium-137 being the most prevalent [4].

Nuclear regulatory committees have adopted risk models based on a linear, no-threshold relationship between radiation dose and risk of cancer [7, 16]. That is, any radiation exposure at all will increase risk of cancer above the baseline, and cancer risk increases linearly with dose; an individual who receives a 0.3 Sievert effective dose in a given time period will be ten times more likely to develop cancer than one who receives 0.03 Sievert in the same time period. The linear, no-threshold model was found to fit existing data well, and is also simple to use and makes conservative risk estimates, encouraging minimal radiation exposure.

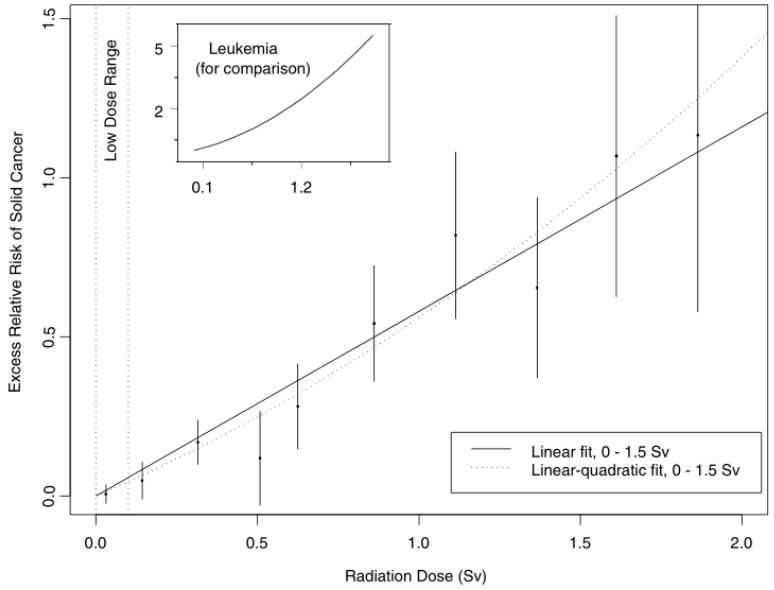

Figure 4 - The excess relative risk of solid cancers for Japanese atomic bomb survivors as calculated by the BEIR VII committee [7]. A linear, no-threshold fit and a linear-quadratic fit are plotted.

As shown in the atomic bomb survivor studies, incidence of cancer varies greatly by organ, with the breast and thyroid showing the greatest excess relative risk (ERR) at a dose of 1 Sv. The overall ERR for solid cancers is 0.63 per Sv: there was 63% greater incidence of solid cancer in the exposed study group than the control group [7].

After taking into account many studies, the International Commission on Radiation Protection (ICRP) developed a stochastic risk model that states that the absorption of 1 Sv of absorbed dose causes 5% increase in cancer risk [9, 20]

Neutron Sources and Energy

Nuclear fission is the most common source of neutron radiation. Fission occurs when unstable nuclei split into excited fragments, from which neutrons "evaporate" as the fragments relax to lower energy states.

Fission

Fission occurs when an atom captures a neutron to become an unstable isotope, and subsequently splits into two daughter atoms. These fragments are sufficiently excited to shed neutrons, beta particles, and gamma rays, just as in spallation. Many neutrons are captured either by other nuclei, continuing the fission reaction. In a reactor, fission products may be captured by absorptive rods to prevent the reaction from going out of control.

Fission reactions produce a good deal of heat, requiring various dissipation processes.

Fast Neutrons

Neutrons with energy greater than 1.0 MeV are characterized as fast neutrons. Most neutrons produced in nuclear processes are fast neutrons. Fast neutrons travel with enough energy that the likelihood of them interacting with other particles is relatively low. Fast neutrons are not likely to be absorbed by a nucleus and continue a fission reaction, for example.

In a fission reactor, moderating materials are used to slow them and enable continuous reactions. Water (in the form of H_2O or D_2O) and graphite are commonly used moderators; the collisions between the neutrons and the similarly-sized nuclei are more likely to result in scattering than absorption. That is, the neutron is likely to remain free, but will be slowed by the collision to thermal and epithermal energy levels, where their capture cross-section is higher, allowing reactions to continue.

Epithermal Neutrons

Many distinctions are made in the range of energies between the fast and thermal neutrons. In general, neutrons with energy between 0.5 eV and 1.0 MeV can be characterized as epithermal. The closer the energy of an incident neutron is to its surroundings, the greater its likelihood of being absorbed into a nucleus.

Thermal Neutrons

Thermal neutrons are in thermal equilibrium with their surroundings, having energies less than 0.5 eV. At a temperature of 290K, a common approximation of room temperature, the corresponding energy of a neutron is 0.025 eV, so this is the value often used for calculations and simulations. Thermal neutrons have the greatest absorption cross section. Fission reactions require the presence of thermal neutrons, which are absorbed by fissile nuclei to start reactions.

Neutron Interaction Cross Section

The probability of a neutron interacting with an atom is dependent on the incident neutron's energy, and also on the atom's microscopic neutron interaction cross section σ. This value, which has units of either cm^2 or barns (one barn equals 10^{-24} cm^2), represents the effective cross sectional area of an atom's nucleus, which is where interaction will occur.

$$\sigma = \pi r^2 \tag{6}$$

In this equation, r is the effective radius of the atom's nucleus.

Depending on the material in question, a neutron may have variable likelihood to either scatter or be absorbed by an atomic nucleus. With this in mind, atoms indeed have separate cross sections for scattering and absorption. The interaction cross section referred to here is the sum of the scattering cross section σ_s and absorption cross section σ_a.

$$\sigma = \sigma_s + \sigma_a \tag{7}$$

On a macroscopic level, the microscopic cross section σ is multiplied by the number density *n* of atoms in the sample in question, yielding a macroscopic cross section Σ:

$$\Sigma = \sigma n \tag{8}$$

In samples composed of a mixture of elements, the interaction cross sections combine simply according to the number density of constituent atoms.

Neutron Activation

Neutron activation refers to the process of exposing a material to a neutron beam, causing the nuclei to capture neutrons and become unstable. This process is highly useful for characterizing the radiation emitted from a neutron source and for identifying the elemental makeup of unknown samples.

Neutron Source Characterization

Neutron activation can be used to measure the fluence rate of neutrons coming from a source. A well-understood material can be exposed to a neutron source for a period of time, activating it. The activity of the material can then be measured and related to the neutron fluence rate.

The activation of a sample is dependent on the fluence rate of the neutron source, and also on the properties of the sample itself. A given nuclide has a neutron capture cross section, which is a numerical representation of how likely it is to absorb a neutron. It is also important to take into account the number of atoms present in a sample.

Of course a sample exposed to a neutron source for a longer time will be more radioactive, since more interactions are allowed to occur. While exposed to a neutron source, activity in the target sample grows according to a saturation factor

$$S = 1 - e^{-\lambda t} \tag{9}$$

where λ is the decay constant of the activated target element, and t_i is the time the sample is irradiated.

Once the sample is removed from the neutron source, the activated nuclides will decay without new ones being made. The activity of a sample cannot be made while the sample is still being activated, so this needs to be taken into account. The decay occurs exponentially, according to a decay factor

$$D = e^{-\lambda t_d} \tag{10}$$

In this equation, λ is again the decay constant and t_d is the length of time the sample is allowed to decay.

The Neutron Activation Equation

The equation relating each of these factors is fairly straightforward:

$$A = N\sigma\varphi(1 - e^{-\lambda t_i})(e^{-\lambda t_d}) \tag{11}$$

where

A	is the activity of the sample
N	is the number of atoms in the sample
σ	is the neutron capture cross section
φ	is the fluence rate of neutrons
λ	is the decay constant of the radioactive isotope
t_i	is the length of time of irradiation
t_d	is the time of decay between activation and count

Neutron Activation Analysis

Neutron activation analysis (NAA) takes advantage of the unique decay patterns of certain common elements in order to identify them in samples of unknown material. While some elements are more detectable in trace amounts than others, up to 74 elements can be identified using NAA with a range of sensistivity between 1 and $1x10^7$ picograms [10].

The nuclei of different elements emit distinct kinds of radiation as they transform back to a stable form. For example, when naturally-occurring and stable gold-197 is exposed to a neutron source, some atoms may absorb neutrons to become gold-198. Gold-198 is unstable and most commonly decays to mercury-198 by emission of a beta particle of energy 0.961 MeV and a gamma ray of energy 0.412 MeV (Figure 5).

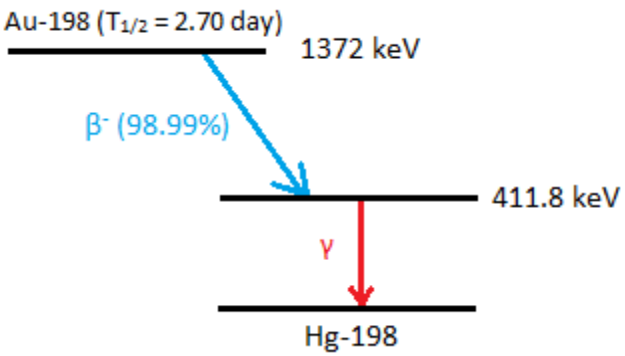

Figure 5 - The decay scheme of gold-198 to stable mercury-198 by beta emission.

No other radioactive element undergoes this same transition. Thus if radiations are collected that indicate that these transitions took place, it is likely that the original sample contained gold-197, which was activated into gold-198 and subsequently decayed.

By activating an unknown sample and measuring its characteristic radiation (specifically the gamma), the elements in the sample can be determined, even when only trace amounts of the materials are present.

Computational Simulation of Radiation

The use of radioactive materials in any practical application requires strict safety procedures and monitoring due to the potentially hazardous and damaging effects radiation can have on the environment. In place of real-life experiments, computer simulations can be used to generate useful information and results for even complicated systems. Simulations have the further benefit of being highly flexible and customizable—the geometry of an experimental setup can be adjusted easily, for example, or a hypothetical part can be modeled that would be impractical to craft for trial testing.

The Monte Carlo Method

In order to create a noticeable effect on the macro scale, the number of particle interactions of a nuclear process must be very large. Furthermore, particle interactions at the atomic level are entirely stochastic. The result is that particle transport can be modeled using a series of probabilities [26].

Monte Carlo N-Particle (MCNP) code models the lifetime of numerous particles in this way. A particle will be produced with characteristics (such as type of particle, energy, and direction) given by the input code. After that, whenever there is a possibility for an event to occur with that particle, the code generates a random number and compares it to known interaction probabilities. These probabilities come from the physical properties of the materials in question, such as interaction cross sections or decay constants. The code follows the initial particle and all subsequent interaction products caused by that particle until they are all absorbed as dose or exit the area of interest (Figure 6).

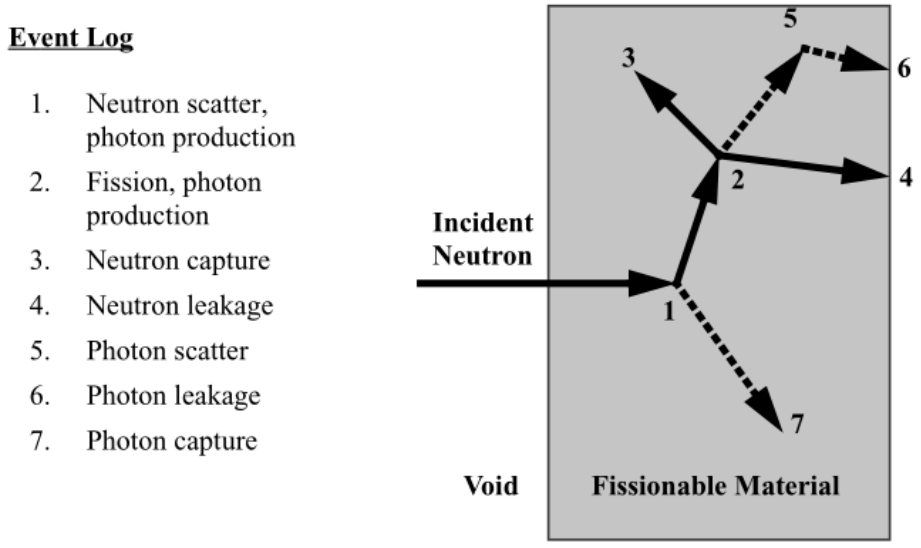

Figure 6 - A possible series of interactions caused by an incident neutron and the order in which they are tracked [26].

By simulating a large number of particles in this way, it is possible to obtain various types of usable information, including current across a surface, particle fluence rate across a surface, or energy deposition within a volume.

Methods

1. Monte Carlo (MCNP) Analysis

i. Determination of Number of Histories

The first geometry used was a series of five concentric one-centimeter-thick spherical tallies spaced six centimeters apart. The tallies were centered on a neutron point source that produced neutrons of energy 0.0253 eV in random directions. The world was filled with air with a composition as defined by the National Institute of Standards and Technology: by weight, 0.000124% carbon, 0.755268% nitrogen, 0.231781% oxygen, 0.012827% argon (NIST). Figure 7 shows the spherical geometry.

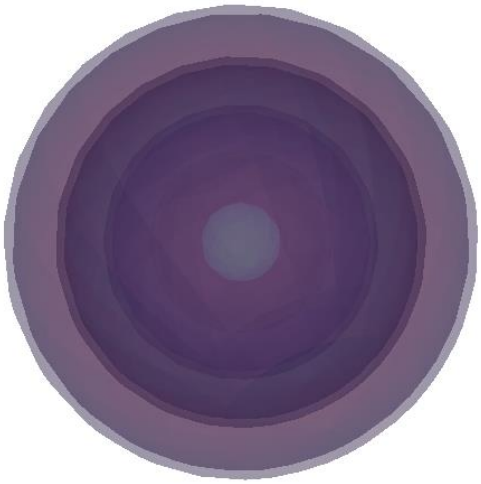

Figure 7 - The spherical geometry used in parts i. and ii. The thinner layers are the tally cells.

The tallies used were F6 dose tallies, which record energy deposition averaged over the cell in units of mega-electron volts per gram (MeV/g). The dose recorded by each tally was not important at this stage, but F6 tallies would be used to full effect later, so it made sense to use them here. Also recorded is the tally error and a figure of merit, both of which provide some insight into how statistically reliable the simulation is. The spherical setup would ensure that the maximum number of particle interactions and the corresponding dose would be recorded at each distance.

This spherical geometry was first used as a stage to determine the number of particles to simulate in order to obtain reliable results. This means that the tallies pass the statistical checks built into MCNP, have a low tally error values, and which have stable figures of merit as a simulation goes on.

Seven simulations were run using the spherical geometry, with the number of particle histories simulated ranging from 10 to 10^7. The results of these simulations can be found in Results section 1.i. An example of the MCNP code with a spherical geometry setup can be found in Appendix N.

ii. Comparison of Geometries

The experiments conducted at UMass Lowell would not have a spherical dosimeter setup; instead the dose readings would be taken by a dosimeter with a relatively small cross-sectional area. In order to better understand the limitations of this setup, simulations with a "linear" setup of dose tallies were performed in MCNP for comparison with the spherical geometry used previously.

In the linear geometry, five one-cubic-centimeter tally cells were placed in a line and spaced six centimeters apart. A disc neutron source of radius six centimeters was placed six centimeters from the first tally cell and produced 0.0253 eV neutrons toward the tallies. As in the spherical geometry, the world was filled with air.

The spherical geometry used in Part i., above, was used as the standard of comparison. Simulations with 10^7 particle histories were run and their results were compared, with regard to absorbed dose and tally error. Figure 8 shows cross-sectional views of both the spherical geometry and the linear geometry.

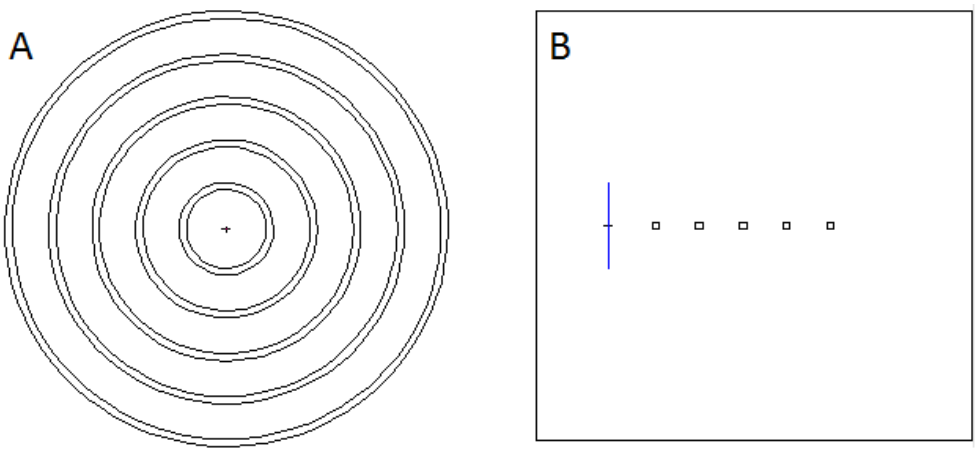

Figure 8 – (A) The spherical geometry, with a central point neutron source. (B) The linear geometry, with disc neutron source (line to the left of the squares).

iii. Effect of Water Backing on Recorded Neutron and Gamma Dose from Thermal and Fast Neutrons

MCNP was used to simulate thermal and fast neutrons and estimate dose for the thermal column and fast neutron facility at UMass Lowell.

This would by simulated by setting up a simple neutron source and placing F6 dose tallies at set distances from it. The tallies were set to record dose from both neutrons and photons, which would be secondary products of particle interactions. Cells containing water would be placed just behind the tally cells, just as solid water blocks would be placed behind dosimeters in the fast neutron dose experiment at the UMass reactor. The thickness of these water cells could be varied and the dose recorded by the tally cells could be plotted and related to the thicknesses.

The neutron source was set at the origin of a 30 x 30 x 2200 cm world filled with the same air used in previous simulations. The source was a disc of radius six centimeters set to emit 0.0253 eV neutrons directly down the x-axis, toward the tally cells. Based on the results of the previous simulations, it was decided that 10^7 particle histories would produce results with low error and stable figures of merit.

F6 neutron/gamma dose tallies were placed at 200 centimeter intervals up to 2000 centimeters. The half-centimeter-square tally cells were backed by cells with two centimeter height and width containing pure light water. The thicknesses of the water cells were 0.1 cm, 1 cm, 4 cm and 10 cm for each respective simulation. Figure 9 shows a tally cell with a four-centimeter backing within the world cell.

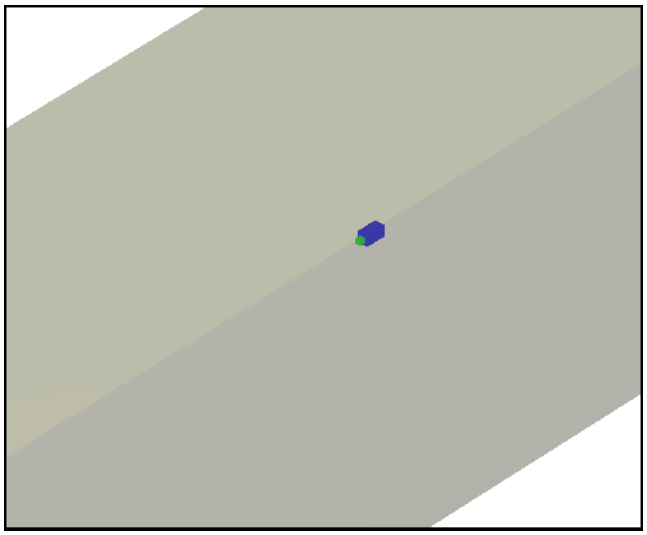

Figure 9 - A tally cell (green) with a 4cm water backing (blue) within the rectangular prism world cell (gray shade).

Since having multiple water cells in a row would cause cumulative shielding effects, it was necessary to run many simulations: ten for each water cell thickness, one at each set distance from the neutron source, with four different thicknesses, for a total of 40 runs. This was achieved easily by utilizing the pStudy perl script that can take one input file with multiple values given for a number of variables, separate it into the required number of standard input files, and then run them individually.

The result of the F6 tallies were dose readings in units of MeV/g. A more common absorbed dose unit is the Gray, equivalent to 1 Joule per kilogram, or 6.241×10^9 MeV/g. The results from the tallies were converted to units of Gray for analysis.

The same simulation was run with the disc neutron source producing “fast” neutrons of energy 1 MeV.

The results of these simulations can be found in Results section 1-iii. The full pStudy input files can be found in Appendix N.

2. Fast Neutron Dose

Upon arrival at the UMass Lowell reactor facility, the Landauer Luxel+ dosimeters (Figure 10) were sorted according to how they would be used. The dosimeter labeled Test was left in an office outside the reactor area to act as a control sample and provide a baseline for background radiation.

Figure 10 - A Luxel+ dosimeter, with pen for scale.

The remaining dosimeters were labeled 1 through 10 and were exposed to radiation from the reactor core in pairs as shown in Table 4. The ninth and tenth dosimeters were left in the control room in the reactor area for the duration of the experiments and could have been used as backups if any stage of the experiment was disrupted.

Table 4 – Reactor power and dosimeter exposure times for the fast neutron irradiation experiment.

Dosimeter Number	Reactor Power Output (watts)	Duration of Exposure (minutes)
1, 2	500	60
3, 4	10 000	10
5, 6	100 000	1
7, 8	1 000 000	0.1

Figure 11 shows two external views of the bunker wherein the dosimeters were exposed to the reactor radiation.

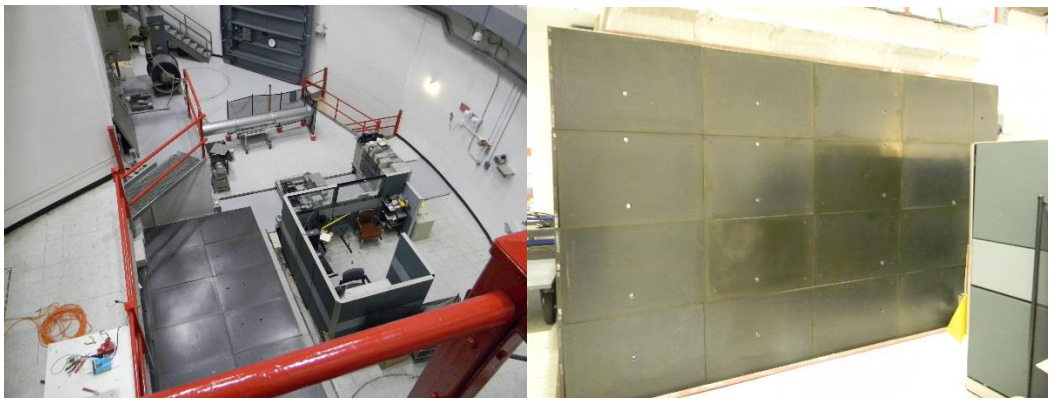

Figure 11 - (Left) An overhead view of the neutron facilities. The thermal column and fast neutron bunker are both visible. (Right) Another external view of the fast neutron bunker. High-density concrete and other insulating materials are used to contain the radiation released within.

A collimation tube, visible in Figure 12, connected this room to the reactor. For each stage of the experiment, the dosimeter pair being used, backed by solid water, would be positioned directly in front of the tube. The dosimeters being used were held in a plastic bag that was affixed to the solid water. While the UMLRR fast neutron irradiation facility has a uniform fluence rate distribution within 10% of the average [24], the dosimeters would get the best results if they were placed in the center of the particle beam, where fluence is most uniform. The bags containing the dosimeters were positioned consistently, using marks on the solid water blocks, to ensure that the dosimeters were in the same location relative to the tube for each stage of the experiment.

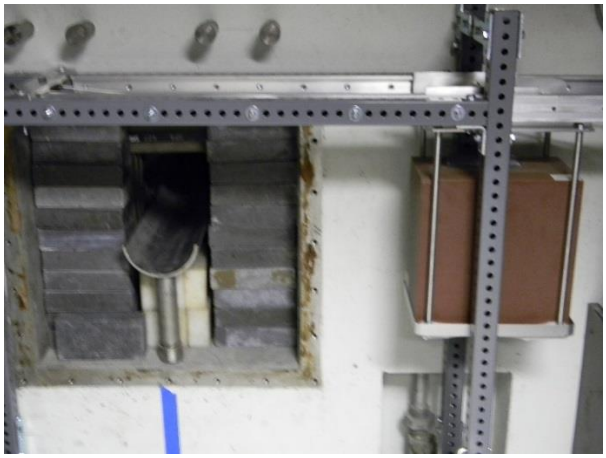

Figure 12 - A picture of the setup inside the bunker. The movable rack system (holding the solid water, right of picture) could be moved from outside the bunker to the front of the collimation tube (left of picture). The tube has a 30cm diameter

In order to position the dosimeters in front of this tube without entering the bunker while it was being irradiated, a movable rack system was used (Figure 13). The 18 centimeters of solid water were set up on a platform which could be moved by a pulley system between the proper position in front of the collimation tube and a location outside the bunker where dosimeters could be affixed to the setup safely. This also made it possible to exchange the dosimeters while keeping the reactor powered up, since raising and lowering the power for each pair of dosimeters would have made the experiment take much longer. A Geiger-Müller counter and a neutron-detecting variant were set up in this area to give indications of the radiation levels there.

Figure 13 - The solid water positioned in front of the collimation tube. The bag containing the dosimeters is held to the solid water blocks by tape.

Once setup was complete, the collimator tube plug was removed and the reactor was run up to a power output of 500 watts. Dosimeters 1 and 2 were affixed to the solid water blocks and moved into position in front of the collimation tube where they were left for a duration of one hour while the power was held constant. After the hour, the dosimeters were removed and the reactor was run up to 10 kilowatts, whereupon dosimeters 3 and 4 were placed in front of the tube for ten minutes. Following this, the reactor was brought up to 100 kilowatts and dosimeters 5 and 6 were put into position for one minute. In the last stage of this experiment, the reactor was brought up to its full power output, 1 megawatt, and dosimeters 7 and 8 were put in place in front of the collimator tube for six seconds before being removed.

When the experiment was concluded, the reactor was powered down and the materials used were collected. The Control dosimeter and dosimeters 1 through 10 were sent to Landauer for processing. Their recorded doses can be seen in Results section 2.

Results

1. Monte Carlo Results

i. Determination of Ideal Number of Histories

Monte Carlo-based MCNP6 code was used to produce and run simulations of a neutron point source surrounded by uniformly spaced spherical tally cells. For each tally distance from the source, the tally error reported by the MCNP software was recorded as the number of histories increased in orders of magnitude from 10 to 10^7. The results were plotted and evaluated to determine the proper number of particle histories to run to obtain significant results in future simulations.

Table 5 - Tally error values by number of histories run for five different tally distances.

Tally Distance (cm) (start of tally shell)	Number of Histories	Tally Error
5.5	1.00E+01	0
	1.00E+02	0.0045
	1.00E+03	0.0053
	1.00E+04	0.0013
	1.00E+05	0.0003
	1.00E+06	0.0001
	1.00E+07	0
11.5	1.00E+01	0
	1.00E+02	0.0058
	1.00E+03	0.0057
	1.00E+04	0.0012
	1.00E+05	0.0005
	1.00E+06	0.0001
	1.00E+07	0
17.5	1.00E+01	0
	1.00E+02	0.0047
	1.00E+03	0.0011
	1.00E+04	0.0011
	1.00E+05	0.0006
	1.00E+06	0.0002
	1.00E+07	0
23.5	1.00E+01	0
	1.00E+02	0.029
	1.00E+03	0.0063
	1.00E+04	0.0013
	1.00E+05	0.0006
	1.00E+06	0.0002
	1.00E+07	0
29.5	1.00E+01	0
	1.00E+02	0.0045
	1.00E+03	0.0016
	1.00E+04	0.001
	1.00E+05	0.0003
	1.00E+06	0
	1.00E+07	0

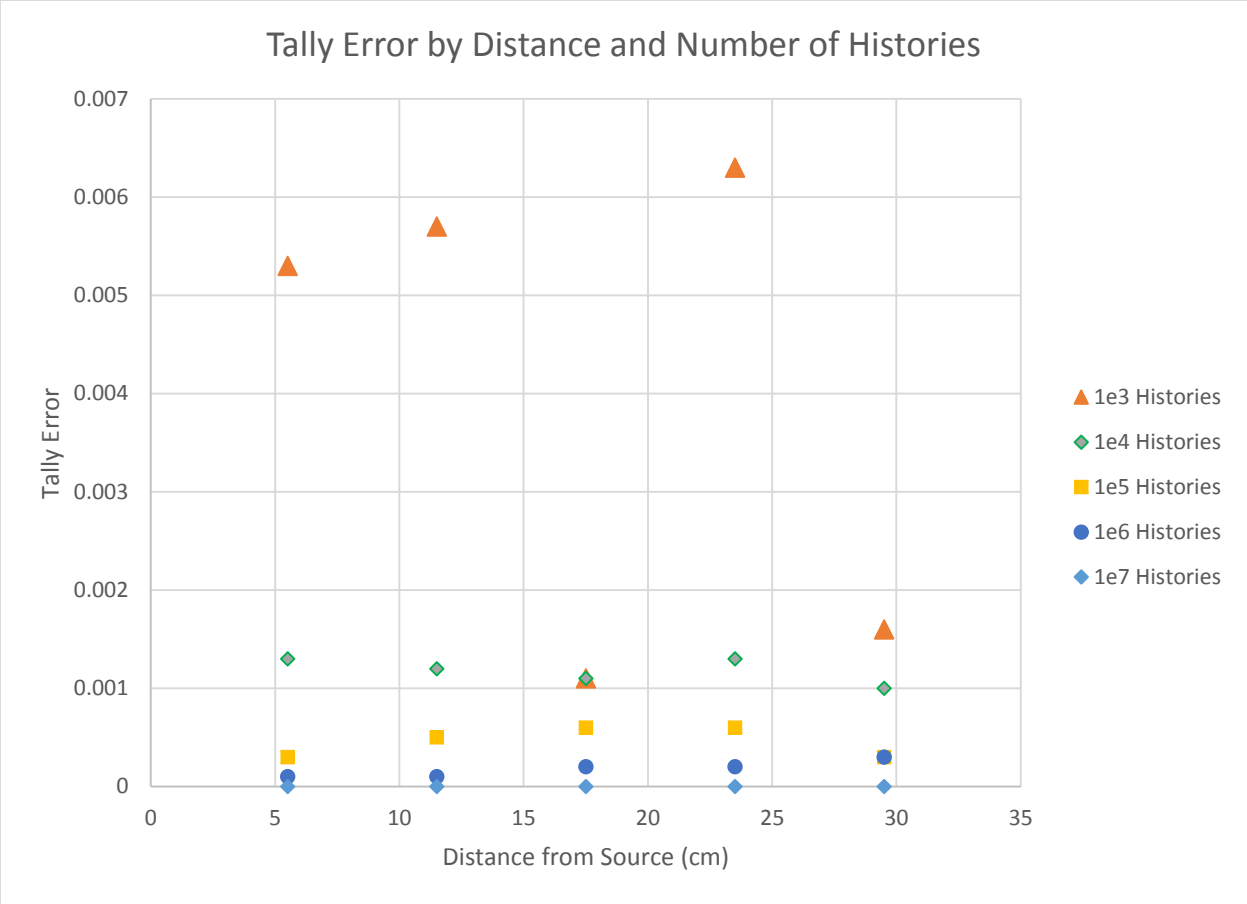

Figure 14 - A plot of reported error at various tally distances by number of histories taken. As the number of histories increases, error decreases. No error is reported at any distance when $1x10^7$ histories were simulated.

Figure 14 shows a plot of the reported error as a function of tally distance from source for many MCNP runs with different numbers of particle histories. The reported error for all tally distances when 10^7 histories are simulated is zero.

ii. Comparison of Geometries

Monte Carlo simulations were run on two tally geometries. The first was a spherical setup with a central neutron point source. The second had a neutron disc source that directed particles toward cubical tallies arranged in a line. The recorded dose and the reported tally error of the two geometries were compared

Table 6 - Dose and tally errors recorded for the spherical and linear setups. 10^7 particle histories were run for each geometry.

Geometry	Tally Distance (front surface) (cm)	Normalized Tally Reading (#/cm²·history)	Tally Error	Particle Fluence (#/cm²)	Error Margin
Spherical	5.5	2.21E-03	0	22115.00	0.00
	11.5	5.55E-04	0	5548.00	0.00
	17.5	2.47E-04	0	2468.20	0.00
	23.5	1.39E-04	0	1387.60	0.00
	29.5	8.86E-05	0	885.56	0.00
Linear	6	8.80E-03	0.0034	87990.00	299.17
	12	8.78E-03	0.0034	87765.00	298.40
	18	8.75E-03	0.0034	87476.00	297.42
	24	8.72E-03	0.0034	87212.00	296.52
	30	8.70E-03	0.0034	86955.00	295.65

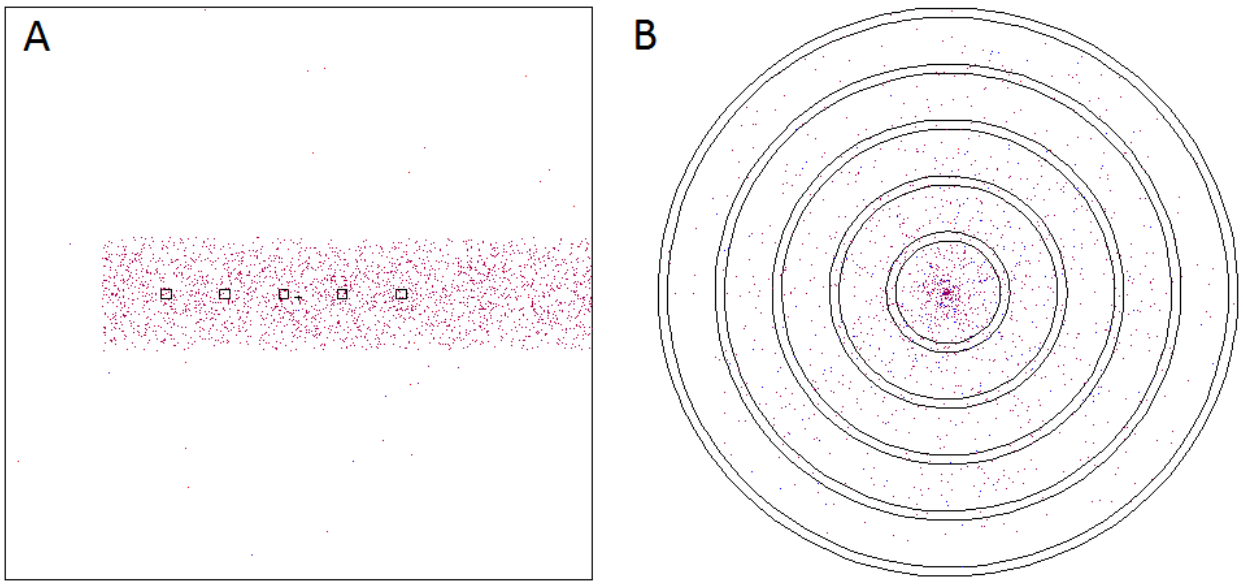

Figure 15 - A hundred-thousand particle sampling of energy depositions in the linear (A) and spherical (B) geometries.

Figure 15 A and B shows the points of energy deposition by a sampling of 100,000 simulated particle histories in the linear and spherical geometries. In the linear geometry, a total of 2,637 interaction points are plotted. In the spherical geometry, a total of 1,619 interaction points.

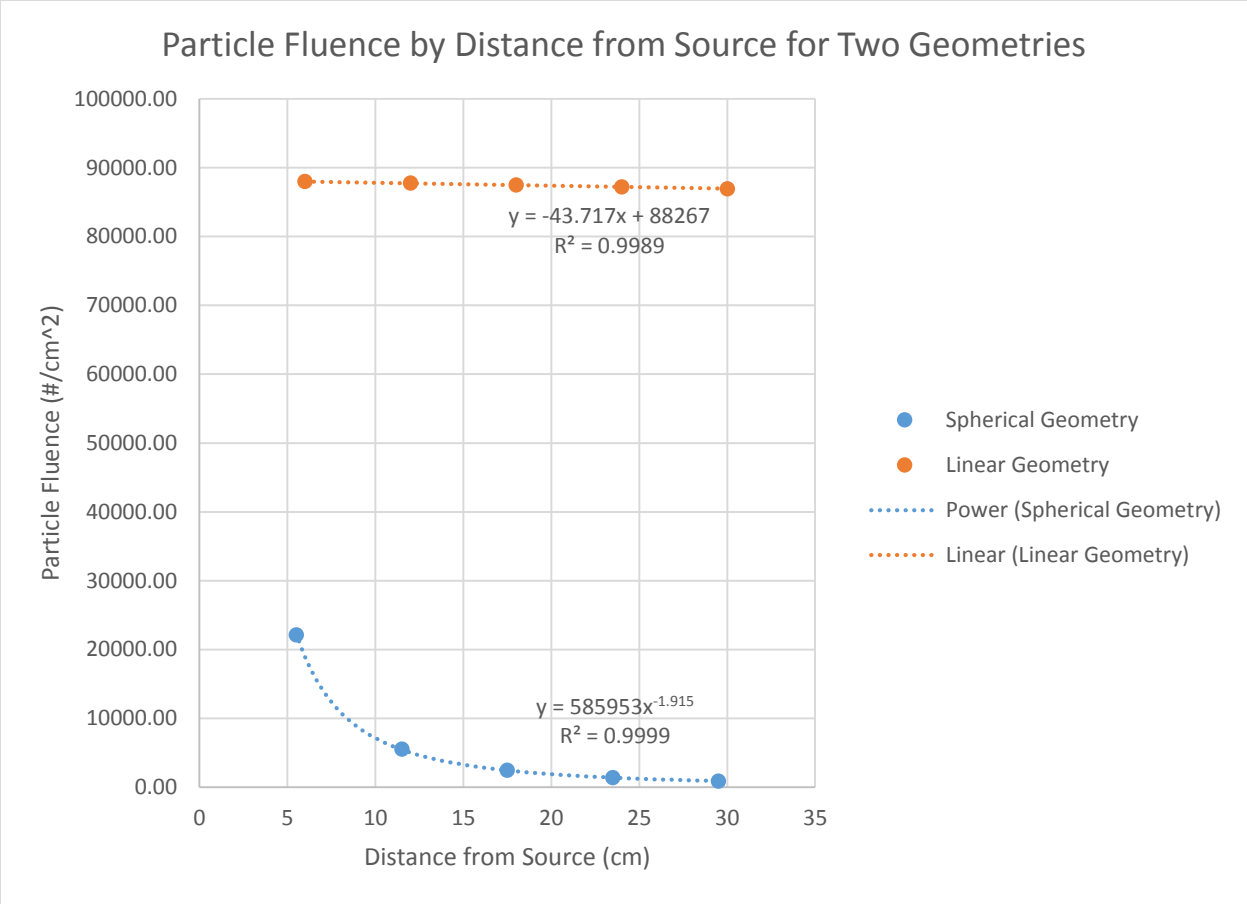

Figure 16 - Plot of the dose recorded by the tallies in the spherical and linear geometry setups. The spherical setup had 0% recorded error; the linear setup had 0.34% error.

The spherical geometry data in Figure 16 follows the equation $D = 3 \times 10^{-13} \cdot x^{-1.915}$, where D is the absorbed dose and x is the distance from the particle source, with an R^2 fit of 0.999. The linear data follows a linear relationship.

iii. Effect of Water Backing on Recorded Neutron and Gamma Dose from Thermal and Fast Neutrons

Table 7 contains selected results from the five MCNP runs of thermal (0.0253 eV) neutrons with tallies positioned in front of water cells of varying thickness, from zero centimeters (no backing) to 10 centimeters. Table 8 contains selected results from the seven runs simulating fast (1 MeV) neutrons. The water cell thickness in the fast neutron simulations varied from zero centimeters to 50 centimeters.

The complete data from the MCNP simulations can be found in Appendix A.

Table 7 – Selected data from the results for thermal (0.0253 eV) neutrons impinging upon a dose tally with a water backing of various thicknesses.

Distance from Source (cm)	**Particle Fluence Through Tally (#/cm^2)**		
	No Backing	*1 cm Backing*	*10 cm Backing*
200	81074	99897	101450
400	73048	90044	91433
600	65856	81177	82449
800	59260	73069	74216
1000	53507	65988	67015
1200	48378	59630	60548
1400	43545	53715	54546
1600	39115	48290	49050
1800	35190	43451	44135
2000	31760	39189	39809

Table 8 - Selected data from the results for fast (1 MeV) neutrons impinging upon a dose tally with a water backing of various thicknesses.

Distance from Source (cm)	**Particle Fluence Through Tally (#/cm^2)**		
	No Backing	*10 cm Backing*	*20 cm Backing*
200	85741	95016	95016
400	82779	91737	91736
600	79847	88483	88483
800	76994	85343	85343
1000	74322	82366	82366
1200	71735	79504	79504
1400	69295	76780	76780
1600	66750	73945	73945
1800	64403	71352	71352
2000	62174	68891	68891

Figure 17 shows the data from the thermal neutron water backing simulations, plotting particle fluence as a function of tally distance from the neutron source. Each set of data comes from a simulation with a different water cell thickness.

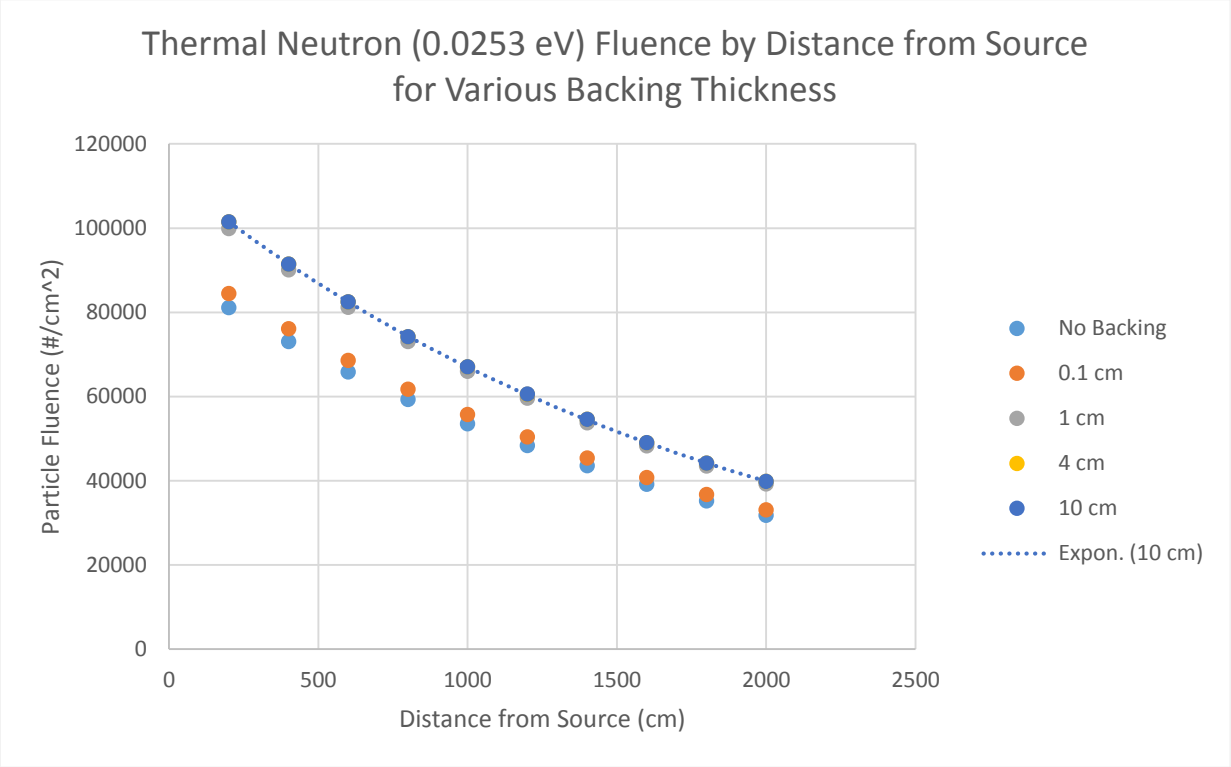

Figure 17 - Plot of particle fluence by distance from source and water backing thickness for thermal neutron simulations.

Figure 17 shows how particle fluence through tallies placed at increasing distance from the thermal neutron source appears to decrease exponentially. At each tally distance, particle fluence increases with the thickness of the water cell behind the tally.

Figure 18 shows the data from the fast neutron water backing simulations. Again, particle fluence is plotted as a function of tally distance from the neutron source.

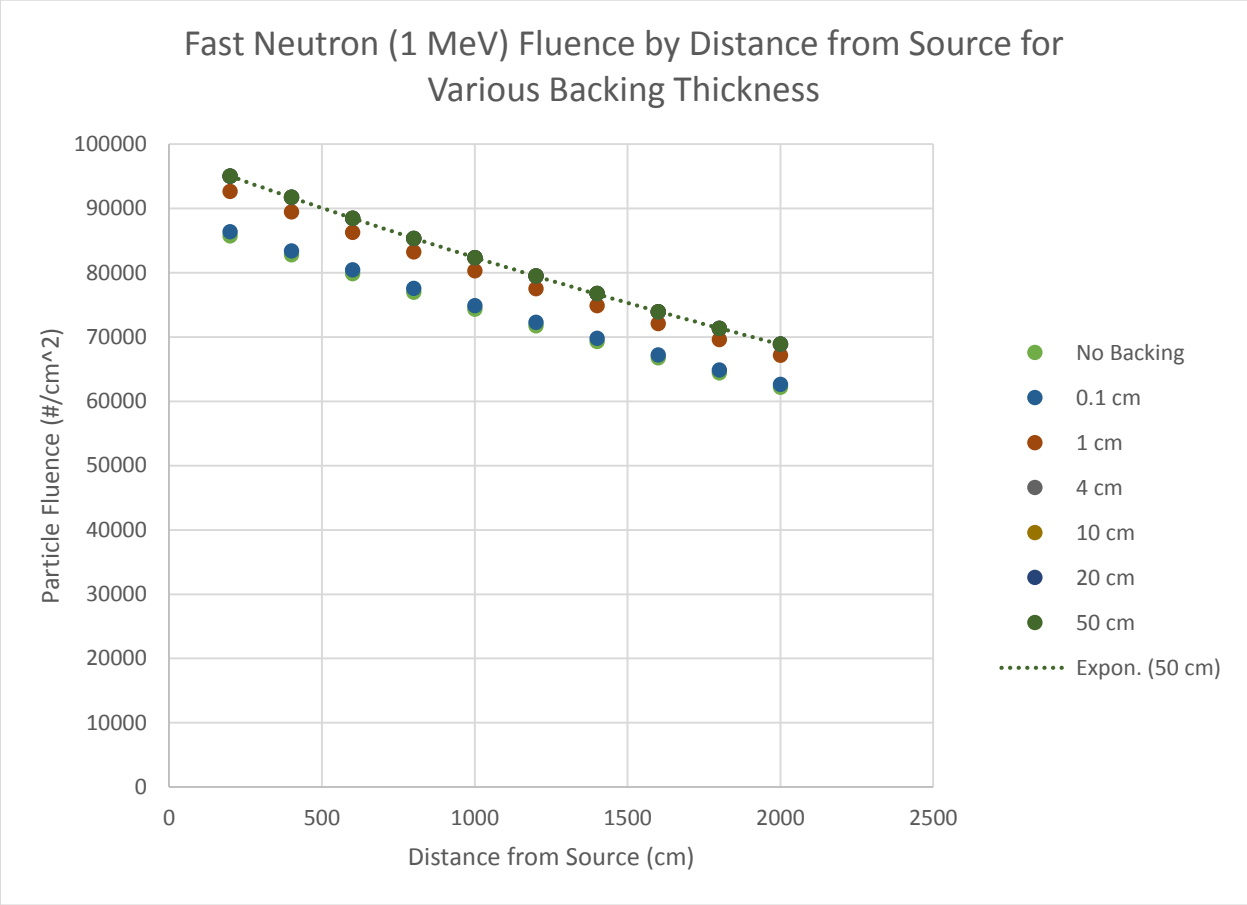

Figure 18 - Plot of particle fluence by distance from source and water backing thickness for fast neutron simulations.

Like in Figure 17, Figure 18 shows that particle fluence appears to decrease exponentially with distance from the neutron source, even with increased neutron energy (1 MeV compared to 0.0253 eV). Again, at each tally distance, particle fluence increases with water backing cell thickness.

2. Fast Neutron Dose Results

Table 9 and Table 10 present the raw and averaged data from the dosimeters used in the fast neutron facility experiment.

Table 9 - Results of dosimetric readings taken at the University of Massachusetts, Lowell Fast Neutron Irradiation facility.

Dosimeter Label	Reactor Power (watts)	Duration of Exposure (minutes)	Photon Dose (cSv)	Photon Dose Rate (cSv/hr)	Neutron Dose (cSv)	Neutron Dose Rate (cSv /hr)	Combined Dose (cSv)	Combined Dose Rate (cSv /hr)
Control	n/a	n/a					0.025	
1	500	60	0.030	0.030	0.580	0.580	0.610	0.610
2	500	60	0.030	0.030	0.580	0.580	0.610	0.610
3	10 000	10	0.090	0.540	1.600	9.600	1.690	10.14
4	10 000	10	0.100	0.600	1.540	9.240	1.640	9.840
5	100 000	1	0.090	5.400	1.390	83.40	1.480	88.80
6	100 000	1	0.100	6.000	1.450	87.00	1.550	93.00
7	1×10^6	0.1	0.140	84.00	2.030	1218.0	2.170	1302.0
8	1×10^6	0.1	0.140	84.00	1.810	1086.0	1.950	1170.0

Table 10 - Combined (neutron and gamma) effective dose rates for each dosimeter and averages by reactor power level.

Reactor Power (Watts)	Exposure Time (minutes)	Combined Effective Dose (Sv)	Combined Effective Dose Rate (CEDR) (Sv/min)	Average CEDR (Sv/min)	CEDR (Sv/hr)	Average CEDR (Sv/hr)
500	60	0.0061	0.000101667	0.000101667	0.0061	0.0061
500	60	0.0061	0.000101667		0.0061	
10 000	10	0.0169	0.00169	0.001665	0.1014	0.0999
10 000	10	0.0164	0.00164		0.0984	
100 000	1	0.0148	0.0148	0.01515	0.888	0.909
100 000	1	0.0155	0.0155		0.93	
1 000 000	0.1	0.0217	0.217	0.206	13.02	12.36
1 000 000	0.1	0.0195	0.195		11.7	

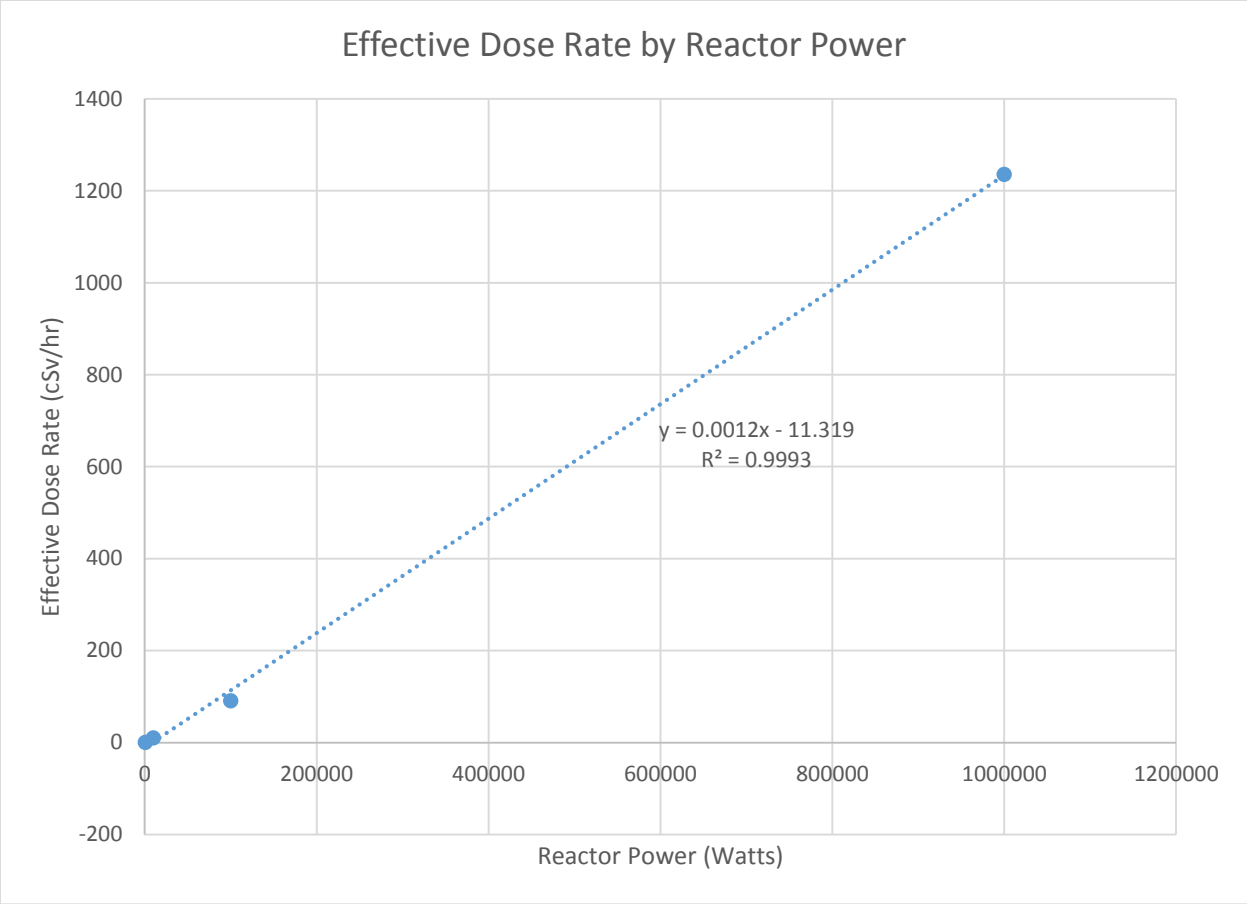

Figure 19 - Plot of effective dose rate as a function of reactor power, showing a linear relationship.

Figure 19 shows a plot of the effective dose rate recorded by the dosimeters as a function of reactor power shows a linear trend between the two, revealing a linear relationship between the two.

The radiation quality factor for high-energy neutrons can be used to calculate the total dose, in gray, delivered to the dosimeters.

Photon Quality Factor (high-energy photons)	1
Neutron Quality Factor (100 keV – 2 MeV)	20

Table 11 - Photon, neutron, and combined dose readings converted to SI units.

Reactor Power (watts)	Duration of Exposure (minutes)	Photon Dose (Gy)	Neutron Dose (Gy)	Combined Dose (Gy)	Combined Dose Rate (Gy/min)
500	60	0.0003	0.00029	0.00059	9.83333E-06
500	60	0.0003	0.00029	0.00059	9.83333E-06
10 000	10	0.0009	0.0008	0.0017	0.00017
10 000	10	0.001	0.00077	0.00177	0.000177
100 000	1	0.0009	0.000695	0.001595	0.001595
100 000	1	0.001	0.000725	0.001725	0.001725
1 000 000	0.1	0.0014	0.001015	0.002415	0.02415
1 000 000	0.1	0.0014	0.000905	0.002305	0.02305

Discussion

In the nuclear industry, the most important tool for combating potentially dangerous mishaps is knowledge: knowledge of how a facility works, what it is capable of, what can go wrong, and how to prevent it. For a facility like the University of Massachusetts, Lowell Research Reactor (UMLRR), which uses radiation directly from the reactor core to perform experiments, safety is a major concern for researchers and workers. By using dosimeters backed by blocks of solid water to simulate a human target, it was possible to estimate the absorbed dose a person could receive while standing in the fast neutron irradiation facility. The results of the dosimetric study were also used to relate reactor power to the fluence rate of particles coming out of the reactor, with the assumption that dose is directly proportional to fluence rate. A similar process could be used to study the output of other, similar reactors around the world.

Prior to performing any experiments at the reactor facilities, it was useful to run computer simulations to see what sort of results could be expected based on the geometry of the experimental setup and the use of solid water phantoms. And before these simulations could be run, simple simulations could be run to see how the program behaved with an ideal setup.

Thus, the first stage of MCNP simulations were finding a suitable threshold for the number of particle histories required to produce results with an acceptable level of uncertainty. It was clear that more histories would provide more stable statistics when working in a Monte Carlo-based simulation environment. With enough histories, eventually the results of a tally will converge to a single number that corresponds to the "true" value of the metric being tallied.

To determine a concrete number of histories at which results have a low uncertainty (and therefore high convergence), seven simulations were performed with the geometry consisting of concentric spherical tallies. This geometry can be seen in Figure 8A. The difference between each simulation was the number of histories recorded, from 10 histories to 10^7 histories, with each recording ten times more than the last. The results of these simulations are recorded in Table 5 and a plot of the data is shown in Figure 14. The results from the runs simulating less than 1000 particles were predictably unusable. However, by evaluating the remaining data, two trends were clear.

First was the relationship between the distance from the particle source and the amount of uncertainty recorded by the software. In the runs with 10^6 and 10^7 histories, the data show a directly proportional relationship between the tally distance and the amount of error. The more distant a tally is from the particle source, the fewer particles would reach the tally volume due to various interactions. With fewer data points to work with, larger uncertainty values were observed in those tallies. The data from the simulation that recorded 1000 histories also suggests this trend, but has some wild fluctuations that call into question their reliability. In the third and fifth tally positions, the tally error reported by the program drops by over 70%. These data points do not follow the trend set by the other three, which show increasing error as the distance from the source increases.

The other useful trend is a decrease in reported tally error as the number of particle histories increases. Error at every distance decreases as the number of histories increases, and the plotted data in Figure 14 shows a large decrease in uncertainty between 1000 histories and 10,000 histories. MCNP reported less than 0.1% error at each tally in the run with 10^7 histories. The spherical geometry has a high efficiency for recording interactions in each tally volume. In less ideal geometries, results with comparably low uncertainty cannot be expected. However, 10^7 histories is a good baseline number for simulating other geometries.

Knowing that real-world experimental circumstances are far less ideal than the concentric sphere tally geometry used to test tally error, the next step in this project was to compare the spherical setup to a more realistic model. A linear geometry was created, with particles directed in the general direction of low-volume dose tallies as shown in Figure 8B.

Particle fluence was recorded in with the spherical geometry decreased with distance approximately according to the inverse-square law, roughly following the equation

$$F = 585953 \cdot x^{-1.915} \tag{12}$$

where F is the particle fluence and x is the distance from the particle source. However, the fluence in the linear geometry appear to follow a more linear relationship, and barely reduce at all.

By running the code for 10^7 histories, the amount of error in the data was found to be very low: less than 0.1% in the spherical setup and 0.34% in the linear setup. This uncertainty is dominated by the inherent uncertainty in the cross-section tables the program uses to model particle interactions, rather than being caused by a lack of statistical convergence. These low error statistics are consistent at each distance from the particle source.

Despite the low uncertainties, there was discrepancy between the two results. The fluence data from the spherical geometry decreases quickly, in an exponential fashion, while the fluence in the linear geometry does not decrease quickly at all. To explain this inconsistency, it is useful to see a visual representation of the simulation. Figure 15 shows the points where energy deposition occurred during a 100,000-history simulation in the linear (A) and spherical (B) geometries.

In the linear geometry, it can be seen that interactions occur with a consistent density down the length of the simulation volume. However, in the spherical geometry, the highest concentration if interactions occur within the first cell, before the 5.5 centimeter radius where the first tally cell begins. Furthermore, there are more total interactions in the linear geometry than in the spherical. There are 2637 points plotted in the linear geometry, while there are only 1619 points plotted in the spherical geometry. The composition and density of the material filling up all of the world cells being equal in both geometries.

The main difference between the two geometries is the particle source. While both produce 0.0253 eV neutrons, the source in the linear geometry is a disc source that directs the particles down the axis of the tallies. The source in the spherical geometry is a point source, and the initial direction of each simulated particle is determined randomly. This difference in source must be the cause of the difference in interaction distribution through the volume of the simulated worlds. While this make it problematic to compare the two geometries directly, it provides a useful result. Since the fluence of particles in the linear geometry does not decrease drastically with distance from the source, a similar result can be expected in the real-world reactor experiment. The collimation tube at the reactor facility will provide a beam of particles similar in nature to the simulated disc source. When the dosimeters are exposed to the particle beam at the reactor, we will not have to worry about a significant drop off in particle fluence due to the distance between the particle source and the dosimeter.

The final series of computational simulation performed in this project evaluated particle fluence through tally volumes using water phantoms located behind each of the tallies in the linear geometry model. This was done with the intention of modeling a dosimeter placed on a human body at various distances from a mono-energetic particle source.

The results from these particle fluence estimations are recorded in Table 7 and Table 8, and are plotted in Figure 17 and Figure 18. The data for both thermal (0.0253 eV) and fast (1 MeV) neutron energies were fit by exponential curves with low uncertainty. In the thermal neutron simulations, it was observed that increasing the backing thickness increases the fluence readings in the tally volume, up to a threshold of around 1 cm. The difference between the 0.1 cm-backing curve and the 1 cm-backing curve is much greater than the difference between the 1 cm-backing curve and the 10 cm-backing curve. Once the backing is about one centimeter thick, any additional thickness will have a minimal effect on the fluence reading.

This threshold effect is a result of the high interaction cross section of low-Z materials such as the hydrogen atoms in water. Low energy neutrons readily interact with these materials within a small penetration depth, leading to elastic scattering or secondary effects such as gamma rays. The interactions cause back scatter of particles, so additional fluence is recorded in the tally. Based on these results, the majority of the neutrons interact inside the first centimeter of the water cell, so maximum back scatter occurs at this thickness. Since few neutrons penetrate further than this, additional thickness will not cause any significant increase in fluence.

In the fast neutron models, results showed that increasing the backing thickness from 0.1 cm to up to 50 cm had a similar effect as in the thermal case, increasing the particle fluence recorded by the tally due to back scatter. Above a threshold thickness, increasing the thickness of the water cell did not increase particle fluence significantly. This threshold is between 10 and 20 centimeters for 1 MeV fast neutrons. Based on these results, a solid water backing of thickness between 10 cm and 20 cm would provide the desired effect of maximizing dose readings in the experiment at the Lowell research reactor. The 18 cm used in the reactor experiments was an acceptable thickness that increased particle backscatter, and therefore dose readings, to a maximum.

Dosimetric readings were taken at the University of Massachusetts, Lowell Fast Neutron Research facilities using neutron and photon dosimeters backed by 18 centimeters of solid water. The reactor was run at four power settings for different lengths of time to obtain absorbed dose and absorbed dose rate information.

Figure 19 shows a plot of the dose rate as calculated from the dosimeter readings as a function of the reactor power. The dose rate increases linearly with reactor power. Increasing the reactor power does not increase the energy of the particles: rather, the increased dose is a result of an increased fluence rate of particles. Thus it is the fluence rate that increases linearly with reactor power. In order to properly relate the dose rate to particle fluence rate, the energy of the particles must be well defined.

While Figure 19 only contains four data points, a linear relationship between reactor power and effective absorbed dose was observed. Further experimental work to more accurately characterize this relationship should include an increased number of evaluated reactor powers.

The dosimeters recorded doses between 0.61 cSv and 2.17 cSv across the various tests. Using a radiation weighting factor of 1 for gamma photons and a weighting factor of 20 for neutrons of energy between 100 keV and 2 MeV, this corresponds to absorbed dose rates between 0.00059 Gy per hour and 1.449 Gy per hour.

At the lowest reactor power of 500 watts, a person standing in the neutron beam would reach their maximum annual dose limit of 0.05 Sv in 490 minutes, or over eight hours. Reaching an annual dose limit in a matter of hours is an overexposure, not one that would lead to the life-threatening symptoms of acute radiation syndrome. However, in the linear no-threshold risk model for stochastic effects introduced by the International Commission on Radiological Protection (ICRP), the risk of cancer increases by 5% per Sievert received [9]. A 0.05 Sv effective dose corresponds to a 0.25% increase in cancer risk—not a huge increase, which is why this is the annual limit, but perhaps a bit intimidating to those who are regularly exposed to radiation.

When the reactor power is 10000 watts, the dosimeters recorded an average of 1.665 cSv in the ten minute exposure time, corresponding to a dose rate of 0.001665 Sv per minute. An individual exposed to this radiation would reach the annual 0.05 Sv limit in 30 minutes. When

the reactor has a power output of 100000 watts, ten times higher, the dose limit would be reached in just over three minutes.

At the highest power level of 1 megawatt, the combined effective gamma and neutron dose rate was around 12.4 Sv per hour, or 0.206 Sv per minute. Being exposed to his dose rate would exhaust the 0.05 Sv recommended dose limit in about 14 seconds. Assuming the highest radiation weighting factor of 20 for neutrons between 100 keV and 2 MeV [17, 20], the dose rate would be close to 1.4 Gy per hour. Subjected to this radiation, an individual would receive a dose that would be expected to kill 50% of an exposed population within 60 days (the $LD_{50/60}$ dose) in around 15 minutes.

Table 12 - Exposure time required to reach significant dose and effective dose. Note the varying units of time.

Reactor Power (Watts)	**Time to 0.05 Sv Effective Dose**	**Time to 0.35 Gy Dose (no treatment $LD_{50/60}$)**
500	8.2 hours	24 days
10 000	30.03 min	33.6 hours
100 000	3.300 min	3.5 hours
1 000 000	14.5 seconds	14.83 min

The high-density concrete and borated polyethylene shielding systems encasing the bunker contains the vast majority of the radiation that is produced and directed down the collimation tube. This shielding allows for outside areas to be classified as low risk; that is, it is as area where an individual will not be at risk of receiving their annual limit of intake of radiation.

The results obtained from these experiments helped evaluate the relationship between reactor power and fluence rate at the UMLRR facility. They also provided valuable information about the absorbed dose risk level of the facility.

This procedure was simple enough to undertake at any reactor with facilities similar to those at UMass Lowell. The use of a solid water phantom to maximize the absorbed dose recorded by the dosimeters resulted in high-quality data that showed a clear linear relationship between reactor power and dose rate.

In a future study, in order to create a more complete picture of the power-dose rate relationship, it is recommended that more dose readings at set intervals of reactor power are taken in order to get more data points.

Based on the work in this study, a further experiment could be to set up a dosimeter in the irradiated bunker area but not directly in the radiation beam to measure the dose an individual could receive from ambient radiation effects. Another possible expansion on this work would be to quantify the relationship between absorbed dose as recorded by the dosimeters and the actual fluence of particles coming out of the reactor. It would also be interesting to carry out the experiment without water backing in order to see how experimental data compares with the data from the Monte Carlo simulation.

Works Cited

[1] *Annual Energy Review 2011*. Rep. no. DOE/EIA-0384(2011). Washington, D.C.: U.S. Energy Information Administration, 2012. Print.

[2] Ashbaker, Eric. *Characterizing the Neutron Spectra in Various Irradiation Facilities within the Oregon State University TRIGA Reactor*. Oregon State University, 24 June 2005. Web. 24 Sept. 2013.

[3] Carpenter, J. M. "Neutron Production, Moderation, and Characterization of Sources." Argonne National Laboratory, 2004. Web. 17 Sept. 2013.

[4] "Chernobyl: Assessment of Radiological and Health Impacts." Nuclear Energy Agency, 2002. Web. 28 Mar. 2014. <https://www.oecd-nea.org/rp/chernobyl/>.

[5] "CR-39 Technology." *Landauer Europe*. N.p., n.d. Web. 1 Oct. 2013.

[6] Hall, Eric J., and Amato J. Giaccia. *Radiobiology for the Radiologist*. Philadelphia: Wolters Kluwer Health/Lippincott Williams & Wilkins, 2012. Print.

[7] *Health Risks from Exposure to Low Levels of Ionizing Radiation: BEIR VII Phase 2*. Washington, D.C.: National Academies, 2006. Print.

[8] Ian S. Anderson, Robert L. McGreevy, Hassina Z. Bilheux; Neutron Imaging and Applications; Springer 2009.

[9] ICRP, 2007. “The 2007 Recommendations of the International Commission on Radiological Protection”. ICRP Publication 103. Ann. ICRP 37 (2-4).

[10] Glascock, Michael D. "Overview of Neutron Activation Analysis." *The Archaeometry Laboratory at the University of Missouri Research Reactor*. University of Missouri, n.d. Web. 10 Feb. 2014. <http://archaeometry.missouri.edu/naa_overview.html>.

[11] “Luxel+ Dosimeter for X, Gamma, Beta, and Neutron Radiation.” *Landauer Europe*. N.p., n.d. Web. 1 Oct. 2013.

[12] "NIST: X-Ray Mass Attenuation Coefficients - Table 2." X-Ray Mass Attenuation Coefficients - Table 2. National Institute of Standards and Technology, n.d. Web. 22 Nov. 2013.

[13] "Part 20 - Standard for Protection Against Radiation." *NRC Regulations: Code 10, Code of Federal Regulations*. 11 March 2014. Web. <http://www.nrc.gov/reading-rm/doc-collections/cfr/part020/>.

[14] "Radiation Weighting Factors." *European Nuclear Society*. N.p., n.d. Web. 13 Jan. 2014. <https://www.euronuclear.org/info/encyclopedia/r/radiation-weight-factor.htm>.

[15] "Radioisotopes in Medicine." World Nuclear Association, Jan. 2014. Web. 3 Feb. 2014. <http://www.world-nuclear.org/info/Non-Power-Nuclear-Applications/Radioisotopes/Radioisotopes-in-Medicine/>.

[16] *Reactor Concepts Manual: Biological Effects of Radiation*. Rep. N.p.: United States Nuclear Regulatory Commission, n.d. Print.

[17] "Relative Biological Effectiveness, Quality Factor, and Radiation Weighting Factor: ICRP Publication 92." *Annals of the ICRP* 33.4 (2003): 1-121. *ScienceDirect*. Web. 3 Mar. 2014. <http://www.sciencedirect.com/science/article/pii/S0146645303000241#>.

[18] *Report of the United Nations Scientific Committee on the Effects of Atomic Radiation 2010: Fifty-seventh Session, Includes Scientific Report, Summary of Low-dose Radiation Effects on Health*. New York: United Nations, 2011. Print.

[19] "Research Reactors." World Nuclear Association, Oct. 2011. Web. 29 Jan. 2014. <http://www.world-nuclear.org/info/Non-Power-Nuclear-Applications/Radioisotopes/Research-Reactors/>.

[20] "Summary of Recommendations." *Annals of the ICRP* 21.1-3 (1991): 67-77. *Sage Journals*. Web. 3 Mar. 2014. <http://ani.sagepub.com/content/21/1-3.toc>.

[21] "Thermoluminescent Dosimeter." *Nondestructive Testing Resource Center*. N.p., n.d. Web. 2 Oct. 2013. <http://www.ndt-ed.org/EducationResources/CommunityCollege/RadiationSafety/radiation_safety_equipment/thermoluminescent.htm>.

[22] Turner, James E. *Atoms, Radiation, and Radiation Protection*. Weinheim: Wiley-VCH, 2007. Print.

[23] Molnar, Zs. "Neutron Activation Analysis." Budapest University of Technology, n.d. Web. 4 Sept. 2013.

[24] "Neutron Facilities." *Radiation Lab: UMass Lowell*. University of Massachusetts Lowell, n.d. Web. 3 Feb. 2014. < http://www.uml.edu/Research/RadLab/Neutron-Facilities.aspx >.

[25] Valentin, J. *The 2007 Recommendations of the International Commission on Radiological Protection*. Oxford, England: Published for the International Commission on Radiological Protection by Elsevier, 2007. Print.

[26] X-5 Monte Carlo Team. *MCNP — A General Monte Carlo N-Particle Transport Code, Version 5 Volume I: Overview and Theory*. N.p.: n.p., 2003. Print. (DIA)

Appendix A: Effect of Water Backing MCNP Simulation Complete Result Tables

Table 13 - Results for thermal neutrons impinging upon a dose tally with no water backing.

Distance from Source (cm)	Normalized Tally Reading (#/cm²·history)	Tally Error	Particle Fluence (#/cm²)	Error Margin
200	8.11E-03	0.0035	81074	283.759
400	7.30E-03	0.0037	73048	270.2776
600	6.59E-03	0.0039	65856	256.8384
800	5.93E-03	0.0041	59260	242.966
1000	5.35E-03	0.0043	53507	230.0801
1200	4.84E-03	0.0046	48378	222.5388
1400	4.35E-03	0.0048	43545	209.016
1600	3.91E-03	0.0051	39115	199.4865
1800	3.52E-03	0.0054	35190	190.026
2000	3.18E-03	0.0056	31760	177.856

Table 14 - Results for thermal neutrons impinging upon a water backing of thickness 0.1 centimeters.

Distance from Source (cm)	Normalized Tally Reading (#/cm²·history)	Tally Error	Particle Fluence (#/cm²)	Error Margin
200	8.45E-03	0.0035	84461	295.6135
400	7.61E-03	0.0037	76105	281.5885
600	6.86E-03	0.0039	68597	267.5283
800	6.17E-03	0.0041	61735	253.1135
1000	5.57E-03	0.0043	55741	239.6863
1200	5.04E-03	0.0045	50397	226.7865
1400	4.54E-03	0.0048	45367	217.7616
1600	4.08E-03	0.0051	40770	207.927
1800	3.67E-03	0.0053	36676	194.3828
2000	3.31E-03	0.0056	33084	185.2704

Table 15 - Results for thermal neutrons impinging upon a water backing of thickness 1 centimeter.

Distance from Source (cm)	Normalized Tally Reading (#/cm^2·history)	Tally Error	Particle Fluence (#/cm^2)	Error Margin
200	9.99E-03	0.0034	99897	339.6498
400	9.00E-03	0.0035	90044	315.154
600	8.12E-03	0.0037	81177	300.3549
800	7.31E-03	0.0039	73069	284.9691
1000	6.60E-03	0.0041	65988	270.5508
1200	5.96E-03	0.0044	59630	262.372
1400	5.37E-03	0.0046	53715	247.089
1600	4.83E-03	0.0048	48290	231.792
1800	4.35E-03	0.0051	43451	221.6001
2000	3.92E-03	0.0054	39189	211.6206

Table 16 - Results for thermal neutrons impinging upon a water backing of thickness 4 centimeters.

Distance from Source (cm)	Normalized Tally Reading (#/cm^2·history)	Tally Error	Particle Fluence (#/cm^2)	Error Margin
200	1.01E-02	0.0033	101450	334.785
400	9.14E-03	0.0035	91432	320.012
600	8.24E-03	0.0037	82448	305.0576
800	7.42E-03	0.0039	74214	289.4346
1000	6.70E-03	0.0041	67014	274.7574
1200	6.05E-03	0.0043	60546	260.3478
1400	5.45E-03	0.0046	54545	250.907
1600	4.91E-03	0.0048	49050	235.44
1800	4.41E-03	0.0051	44134	225.0834
2000	3.98E-03	0.0054	39808	214.9632

Table 17 – Results for thermal neutrons impinging upon a water backing of thickness 10 centimeters.

Distance from Source (cm)	Normalized Tally Reading (#/cm²·history)	Tally Error	Particle Fluence (#/cm²)	Error Margin
200	1.01E-02	0.0033	101450	334.785
400	9.14E-03	0.0035	91433	320.0155
600	8.24E-03	0.0037	82449	305.0613
800	7.42E-03	0.0039	74216	289.4424
1000	6.70E-03	0.0041	67015	274.7615
1200	6.05E-03	0.0043	60548	260.3564
1400	5.45E-03	0.0046	54546	250.9116
1600	4.91E-03	0.0048	49050	235.44
1800	4.41E-03	0.0051	44135	225.0885
2000	3.98E-03	0.0054	39809	214.9686

Table 18 - Results for fast neutrons impinging upon a dose tally with no water backing.

Distance from Source (cm)	Normalized Tally Reading (#/cm²·history)	Tally Error	Particle Fluence (#/cm²)	Error Margin
200	8.57E-03	0.0034	85741	291.5194
400	8.28E-03	0.0035	82779	289.7265
600	7.98E-03	0.0035	79847	279.4645
800	7.70E-03	0.0036	76994	277.1784
1000	7.43E-03	0.0037	74322	274.9914
1200	7.17E-03	0.0037	71735	265.4195
1400	6.93E-03	0.0038	69295	263.321
1600	6.68E-03	0.0039	66750	260.325
1800	6.44E-03	0.0039	64403	251.1717
2000	6.22E-03	0.004	62174	248.696

Table 19 – Results for fast neutrons impinging upon a water backing of thickness 0.1 centimeters.

Distance from Source (cm)	Normalized Tally Reading (#/cm^2·history)	Tally Error	Particle Fluence (#/cm^2)	Error Margin
200	8.64E-03	0.0034	86372	293.6648
400	8.34E-03	0.0035	83387	291.8545
600	8.04E-03	0.0035	80434	281.519
800	7.76E-03	0.0036	77561	279.2196
1000	7.49E-03	0.0037	74869	277.0153
1200	7.23E-03	0.0037	72270	267.399
1400	6.98E-03	0.0038	69805	265.259
1600	6.72E-03	0.0039	67237	262.2243
1800	6.49E-03	0.0039	64868	252.9852
2000	6.26E-03	0.004	62620	250.48

Table 20 - Results for fast neutrons impinging upon a water backing of thickness 1 centimeter.

Distance from Source (cm)	Normalized Tally Reading (#/cm^2·history)	Tally Error	Particle Fluence (#/cm^2)	Error Margin
200	9.26E-03	0.0034	92646	314.9964
400	8.94E-03	0.0034	89441	304.0994
600	8.63E-03	0.0035	86294	302.029
800	8.32E-03	0.0036	83224	299.6064
1000	8.03E-03	0.0036	80308	289.1088
1200	7.75E-03	0.0037	77525	286.8425
1400	7.49E-03	0.0038	74869	284.5022
1600	7.21E-03	0.0038	72109	274.0142
1800	6.96E-03	0.0039	69586	271.3854
2000	6.72E-03	0.004	67177	268.708

Table 21 - Results for fast neutrons impinging upon a water backing of thickness 4 centimeters.

Distance from Source (cm)	Normalized Tally Reading (#/cm^2·history)	Tally Error	Particle Fluence (#/cm^2)	Error Margin
200	9.50E-03	0.0033	94979	313.4307
400	9.17E-03	0.0034	91700	311.78
600	8.85E-03	0.0035	88451	309.5785
800	8.53E-03	0.0035	85310	298.585
1000	8.23E-03	0.0036	82332	296.3952
1200	7.95E-03	0.0037	79474	294.0538
1400	7.68E-03	0.0037	76752	283.9824
1600	7.39E-03	0.0038	73919	280.8922
1800	7.13E-03	0.0039	71329	278.1831
2000	6.89E-03	0.0039	68868	268.5852

Table 22 - Results for fast neutrons impinging upon a water backing of thickness 10 centimeters.

Distance from Source (cm)	Normalized Tally Reading (#/cm^2·history)	Tally Error	Particle Fluence (#/cm^2)	Error Margin
200	9.50E-03	0.0033	95016	313.5528
400	9.17E-03	0.0034	91737	311.9058
600	8.85E-03	0.0035	88483	309.6905
800	8.53E-03	0.0035	85343	298.7005
1000	8.24E-03	0.0036	82366	296.5176
1200	7.95E-03	0.0037	79504	294.1648
1400	7.68E-03	0.0037	76780	284.086
1600	7.39E-03	0.0038	73945	280.991
1800	7.14E-03	0.0039	71352	278.2728
2000	6.89E-03	0.0039	68891	268.6749

Table 23 - Results for fast neutrons impinging upon a water backing of thickness 20 centimeters.

Distance from Source (cm)	Normalized Tally Reading (#/cm^2·history)	Tally Error	Particle Fluence (#/cm^2)	Error Margin
200	9.50E-03	0.0033	95016	313.5528
400	9.17E-03	0.0034	91736	311.9024
600	8.85E-03	0.0035	88483	309.6905
800	8.53E-03	0.0035	85343	298.7005
1000	8.24E-03	0.0036	82366	296.5176
1200	7.95E-03	0.0037	79504	294.1648
1400	7.68E-03	0.0037	76780	284.086
1600	7.39E-03	0.0038	73945	280.991
1800	7.14E-03	0.0039	71352	278.2728
2000	6.89E-03	0.0039	68891	268.6749

Table 24 - Results for fast neutrons impinging upon a water backing of thickness 50 centimeters.

Distance from Source (cm)	Normalized Tally Reading (#/cm^2·history)	Tally Error	Particle Fluence (#/cm^2)	Error Margin
200	9.50E-03	0.0033	95016	313.5528
400	9.17E-03	0.0034	91736	311.9024
600	8.85E-03	0.0035	88483	309.6905
800	8.53E-03	0.0035	85343	298.7005
1000	8.24E-03	0.0036	82366	296.5176
1200	7.95E-03	0.0037	79504	294.1648
1400	7.68E-03	0.0037	76780	284.086
1600	7.39E-03	0.0038	73945	280.991
1800	7.14E-03	0.0039	71352	278.2728
2000	6.89E-03	0.0039	68891	268.6749

Appendix B: MCNP Decks

Spherical Geometry

Used in determining number of histories to run and to compare to the linear geometry model (Methods sections 1-i. and 1-ii.).

```
PC30 Unblocked Thermal Neutrons, Spherical
c *****GEOMETRY
c
c         z-axis
c           ^
c           |
c
c
c           _
c              \\      \\    \\    \\    \\
c           X   ||      ||    ||    ||    ||      --> x-axis
c           _  //      //    //    //    //
c
c
c  X - point source of thermal neutrons, 0.0253 eV
c  | - ring tallies, 6cm apart. Five total tallies
c
c
c
c
c ***** CELLS
c X05 cells are tally cells; X00 are not. All filled with air, density
1.205e-3 g/cm3
100 1 -1.205e-3 -11    IMP:N=1
105 1 -1.205e-3 11 -12 IMP:N=1
200 1 -1.205e-3 12 -13 IMP:N=1 $density -1.205e-3 g/cm3
205 1 -1.205e-3 13 -14 IMP:N=1
300 1 -1.205e-3 14 -15 IMP:N=1
305 1 -1.205e-3 15 -16 IMP:N=1
400 1 -1.205e-3 16 -17 IMP:N=1
405 1 -1.205e-3 17 -18 IMP:N=1
500 1 -1.205e-3 18 -19 IMP:N=1
505 1 -1.205e-3 19 -99 IMP:N=1
999 0           99     IMP:N=0

c ***** SURFACE CARDS
c all surfaces are spheres centered on origin (SO) with radius specified
11 SO 5.5
12 SO 6.5
13 SO 11.5
14 SO 12.5
15 SO 17.5
```

```
16 SO 18.5
17 SO 23.5
18 SO 24.5
19 SO 29.5
99 SO 30.5     $end of world

c ***** DATA CARDS
MODE N
c
c Source definition SDEF
c SDEF POS=000 CEL=1 ERG=0.34eV WGT=1 TME=0 PAR=1 is complete card. More
concise:
SDEF POS=0 0 0 ERG=2.53e-8
c
c Tally Cards
F06:N 105
F16:N 205
F26:N 305
F36:N 405
F46:N 505
c
c Material Cards: ZZZAAA
M1 & $ Air (C:-0.000124, N:-0.755268, O:-0.231781, Ar:-0.012827) [NIST]
6000.70c -0.000124 &
7014.70c -0.752290 &
7015.66c -0.002977 &
8016.70c -0.231688 &
8017.70c -0.000094 &
18000.59c -0.012827
c
c Cutoff
NPS 10000000 $Stop after 1000000 histories taken
```

Linear Geometry

The code that was used when comparing linear and spherical geometries (Methods section 1-ii.).

```
PC10 Unblocked Thermal Neutrons, Linear
c ***** CELL CARDS
c GEOMETRY
c         z-axis
c           ^
c           |
c
c
c           X
c           X
c           X
```

```
c    disc   X     T      T      T      T      T   --> x-axis
c   source  X            F6
c           X<6cm>      tally
c           X
c
c X - disc source of thermal neutrons (0.0253 eV)
c T - F6 dose tallies, 5 total, 6cm apart
c
c
c
c
c ***** CELLS
1 1  -1.205e-3  17 18 19 20 21 -99    IMP:N=1 $box containing tallies (world)
2 1  -1.205e-3  -17                   IMP:N=1 $ Importance of cell for
neutrons
3 1  -1.205e-3  -18                   IMP:N=1
4 1  -1.205e-3  -19                   IMP:N=1
5 1  -1.205e-3  -20                   IMP:N=1
6 1  -1.205e-3  -21                   IMP:N=1
7 0             99                    IMP:N=0 $IMP=0 means ignore, history
ends in this cell $void outside world

c ***** SURFACE AND MACROBODY CARDS
17 RPP 6 7 -.5 .5 -.5 .5
18 RPP 12 13 -.5 .5 -.5 .5
19 RPP 18 19 -.5 .5 -.5 .5
20 RPP 24 25 -.5 .5 -.5 .5
21 RPP 30 31 -.5 .5 -.5 .5
99 RPP -10 50 -30 30 -30 30  $end of world

c ***** DATA CARDS
MODE N
c
c VOL 8e6 1 1 1 1 1
c Source definition SDEF
c disc source on surface 1 centered on point (0,0.5,0.5) (POS)
c [with 0 extension (EXT) along x-axis (1,0,0) (AXS)]
c radius is 6(units unsure, cm?), particle type is neutrons, energy 0.0253eV
SDEF POS=0 0 0 RAD=d1 PAR=1 AXS=1 0 0 VEC=1 0 0 DIR=1 ERG=2.53e-8
SI1 0 6   $source information card. 1=neutrons, 0=rmin, 6=rmax
SP1 -21 1 $source probability card. Unsure if necessary
c
c Tally Cards
F016:N 2
F026:N 3
F036:N 4
F046:N 5
F056:N 6
c
c Material Cards: ZZZAAA (no materials in this problem)
c From http://physics.nist.gov/PhysRefData/XrayMassCoef/tab2.html
M1 & $ Air (C:-0.000124, N:-0.755268, O:-0.231781, Ar:-0.012827) [NIST]
6000.70c -0.000124 &
```

```
7014.70c -0.752290 &
7015.66c -0.002977 &
8016.70c -0.231688 &
8017.70c -0.000094 &
18000.59c -0.012827
c
c Cutoff
NPS 10000000 $Stop after 10000000 histories taken
```

Water Backing pStudy Deck

For studying different thicknesses of water backing behind dose tallies (Methods section 1-iii.). The values of "WE" are changed to look at different water thicknesses—in this case, the thickness is 0.1 cm. This code was used in both thermal and fast neutron simulations; only the source energy (highlighted) is different.

```
WS10 pStudy deck for comparing water backing thickness
c @@@ OPTIONS = -inner
c @@@ OPTIONS = -jobdir THERMAL
c @@@ OPTIONS = -job inp.txt
c @@@ OPTIONS = -case PONE
c @@@ TS = 200 400 600 800 1000 1200 1400 1600 1800 2000
c @@@ TE = 201 401 601 801 1001 1201 1401 1601 1801 2001
c @@@ WS = 201 401 601 801 1001 1201 1401 1601 1801 2001
c @@@ WE = 201.1 401.1 601.1 801.1 1001.1 1201.1 1401.1 1601.1 1801.1 2001.1
c          ^^^ Change these numbers for different backing thickness
c
c
c ***** DESCRIPTION
c
c GOAL: To determine how varying thickness of water cells affects the dose
detected in front of the water cell at varying distances
c         from neutron source.
c
c A disc source uniformly produces thermal (0.0253 eV) neutrons.
c F6 tally detects neutron and photon dose in MeV/g. Position of tally is
varied to see how dose drops off with distance.
c Tally cell is backed by water cell, density 1. g/cm^3. Thickness of water
cell is 0.1 cm
c World otherwise filled with air, density 1.205e-3 g/cm^3 .
c
c
c
c ***** CELL CARDS
01 1  -1.205e-3  170 175 550 -999     IMP:N,P=1  $ box containing tallies
(world)
02 1  -1.205e-3  -170                 IMP:N,P=1  $ Tally cell
```

```
c 07 2  -8.65      -550                IMP:N,P=1  $ cadmium screen (uncomment
to use)
07 1  -1.205e-3  -550                 IMP:N,P=1  $ no cadmium screen
08 3 -1 -175                           IMP:N,P=1  $ Water backing cell
c
99 0             999                   IMP:N,P=0  $IMP=0 means ignore, history
ends in this cell $void outside world

c ***** SURFACE AND MACROBODY CARDS
170 RPP TS TE -.5 .5 -.5 .5    $ tally box (1x1x1 cm)
175 RPP WS WE -1 1 -1 1      $ water box (0.5x2x2 cm)
c
550 RPP 1 1.1 -20 20 -20 20       $box for cadmium screen (if used)
999 RPP -10 2200 -30 30 -30 30      $end of world

c ***** DATA CARDS
MODE N P $ Neutrons and created photons considered
c
c VOL 8e6 1 1 1 1 1
c Source definition SDEF
c disc source on surface 1 centered on point (0,0,0) projecting down x-axis
c radius is 6cm; particle type is neutrons, energy 0.0253eV
SDEF POS=0 0 0 RAD=d1 PAR=1 AXS=1 0 0 VEC=1 0 0 DIR=1 ERG=2.53e-8
SI1 0 6   $ Full area of disc, rmin=0 rmax=6 cm, produces neutrons
SP1 -21 1 $ Uniform distribution of neutrons produced by source
c
c Tally Cards
F016:N,P 02
c
c
c
c Physics mode: 1 MeV limit energy;
c PHYS:P  1  0  0  0  1
c
c
c
c Material Cards: ZZZAAA (no materials in this problem)
c From http://physics.nist.gov/PhysRefData/XrayMassCoef/tab2.html
M1 & $ Air (C:-0.000124, N:-0.755268, O:-0.231781, Ar:-0.012827) [NIST]
6000.70c -0.000124 &
7014.70c -0.752290 &
7015.66c -0.002977 &
8016.70c -0.231688 &
8017.70c -0.000094 &
18000.59c -0.012827
c
M3 1001.70c   0.6667   8016.70c   0.3333        $ Water
c
c Cutoff
NPS 10000000
```